

# IMPROVING SMOOTHED AGGREGATION AMG ROBUSTNESS ON STRETCHED MESH APPLICATIONS\*

CHRISTOPHER M. SIEFERT<sup>†</sup>, RAYMOND S. TUMINARO<sup>‡</sup>, AND DANIEL J. SUNDERLAND<sup>§</sup>

**Abstract.** Strength-of-connection algorithms play an essential role within algebraic multigrid (AMG). Specifically, the strength-of-connection scheme determines which matrix nonzeros are classified as *weak* and so ignored when coarsening matrix graphs and defining sparsity patterns for interpolation. The general goal is to encourage coarsening only in directions where error can be smoothed and to also avoid coarsening across sharp problem variations. Unfortunately, developing robust, practical, and inexpensive strength-of-connection schemes is extremely challenging.

The classification of matrix nonzeros involves four distinct aspects: (a) choosing a strength-of-connection matrix, (b) scaling its values, (c) choosing a criterion to classify the scaled values as either *strong* or *weak*, and (d) dropping weak entries which includes adjusting matrix values to account for dropped terms. Typically, smoothed aggregation AMG uses the linear system being solved as the strength-of-connection matrix. It scales these values symmetrically using the square-root of the matrix diagonal. It classifies based on whether scaled values are above or below a user-supplied threshold. Finally, it adjusts matrix values by modifying the diagonal so that the sum of entries within each row of the dropped matrix matches the sum of the original. While these procedures often work well, we illustrate stretched mesh failure cases that motivate alternatives to improve robustness. The first alternative uses a distance Laplacian strength-of-connection matrix. The second idea centers on non-symmetric scaling algorithms. We then investigate alternative classification criteria based on identifying a significant gap in the values of the scaled entries. Finally, an alternative lumping procedure is proposed where row sums are preserved by modifying all retained matrix entries (as opposed to just diagonal entries). A series of numerical results is given to illustrate algorithm trade-offs demonstrating in some cases notably more robust convergence on matrices coming from linear finite elements on stretched meshes.

**Key words.** smoothed aggregation, algebraic multigrid, strength of connection, distance Laplacian

**AMS subject classifications.** 65N55,65F08

**1. Introduction.** Algebraic multigrid (AMG) [4, 20] is a popular solver for large, sparse linear systems. The main idea is to employ coarse problems to accelerate convergence by leveraging the fact that simple relaxation schemes effectively damp error components whose  $A$ -norm is *relatively* large<sup>1</sup>, and so errors that remain after relaxation have relatively small  $A$ -norm. Ideally, these small  $A$ -norm components are smooth and can be well approximated on a lower resolution mesh. Thus, one projects

---

\*Submitted to the editors 2/2026.

**Funding:** This work was partially supported by the Laboratory Directed Research and Development program (Project 236939). Tuminaro was also partially supported by the U.S. Department of Energy, Office of Science, Office of Advanced Scientific Computing Research, Applied Mathematics program. Sandia National Laboratories is a multimission laboratory managed and operated by National Technology and Engineering Solutions of Sandia, LLC, a wholly owned subsidiary of Honeywell International, Inc., for the U.S. Department of Energy's National Nuclear Security Administration under grant DE-NA-0003525. This paper describes objective technical results and analysis. Any subjective views or opinions that might be expressed in the paper do not necessarily represent the views of the U.S. Department of Energy or the United States Government.

<sup>†</sup>Scalable Algorithms Department, Sandia National Laboratories, Albuquerque, NM ([csiefer@sandia.gov](mailto:csiefer@sandia.gov), <https://www.sandia.gov/-csiefer/staff/chris-siefert>)

<sup>‡</sup>Computational Mathematics Department, Sandia National Laboratories, Livermore, CA ([rstumin@sandia.gov](mailto:rstumin@sandia.gov), <https://www.sandia.gov/CCR/staff/raymond-s-tuminaro>)

<sup>§</sup>Sunderland Development, Salem, Oregon. [dan@sunderland.site](mailto:dan@sunderland.site)

<sup>1</sup>The  $A$ -norm of a vector  $v$  is given by  $\sqrt{v^T A v}$  where  $A$  is the positive-definite symmetric matrix that one is interested in solving.

a correction equation to the next coarsest mesh and recursively repeats the process of relaxation (damping oscillatory errors relative to the mesh resolution) followed by further projection. In many cases, however, some oscillatory error components may have small  $A$ -norm that is difficult to damp. As is well known (e.g., see [14]), this issue arises with either anisotropic partial differential equations (PDEs) or isotropic PDEs that are discretized on stretched meshes. Intuitively, most relaxation schemes primarily smooth error in dominant directions. In the mesh-stretching case, these would be directions where grid points are relatively close to each other. To avoid convergence degradation, either special relaxation schemes must be devised (e.g., line relaxation on structured grids) to damp some oscillatory error components or instead coarsening must not occur in directions where errors are oscillatory after relaxation. Most AMG algorithms adopt the later strategy, which we also target in this paper.

While anisotropic challenges have been studied, a robust multigrid algorithm remains elusive for applications that employ unstructured meshes. Earlier anisotropic multigrid research focused on structured grid approaches (e.g. [9, 10, 11, 22]) usually employing semi-coarsening ideas sometimes in conjunction with line/plane relaxation. However, for more general meshes there are usually no lines or planes to leverage (see [16] for some unstructured adaptations). Overall, the most significant unstructured mesh impediment is that of detecting the directions where coarsening should be restricted, as doing this robustly can be computationally expensive. Most techniques [2, 3, 5, 6, 7, 8, 15, 18] employ some kind of analysis phase to discover directions where relaxation struggles to smooth errors. Not surprisingly, the more robust techniques are also generally fairly costly. Instead, most popular AMG codes rely on simple heuristics that attempt to inexpensively infer coarsening directions from matrix coefficients. While these heuristics frequently work, they fail all too often. In this paper, we illustrate cases where smoothed aggregation AMG (SA) [26, 27] fails in the context of stretched meshes. Our focus on stretched meshes (as opposed to anisotropic PDEs) is motivated by applications where anisotropic behavior frequently arises from stretched meshes. Further, we concentrate on matrices produced via first-order finite elements as these are heavily used by scientists. Finally, while we examine Poisson problems, many of our example meshes come from complex applications (e.g., fluid flow or Maxwell's equations), which commonly rely on Poisson-like sub-solves or which give rise to similar issues.

In the smoothed aggregation context, the standard heuristics for anisotropic applications rely on strength-of-connection ideas that were originally introduced for classical AMG [4, 20]. The basic strategy encourages coarsening in preferential directions by dropping entries from the matrix used within the algorithm's coarsening and interpolation construction phases. In this paper, we take a somewhat different perspective on the dropping procedure in that we highlight the four independent individual sub-steps that together determines the process. The first defines a strength-of-connection (SOC) matrix that is used in the classification process. Normally, this is taken as the original system  $A$  that is being solved, but one could instead define a matrix with the same sparsity pattern as  $A$  but different values for the entries. The second sub-step scales the SOC matrix entries so that each scaled entry reflects a relative size as opposed to the absolute sizes of the unscaled system. In smoothed aggregation a symmetric scaling employing the matrix diagonal is normally used. The third sub-step applies a criterion that examines the scaled entries and determines whether this entry should be kept or dropped (because it is strong or weak). The fourth sub-step adjusts the dropped matrix so that it retains some properties of the original matrix. The standard smoothed aggregation procedure simply alters the matrix diagonal of

the dropped matrix so that the row sum (i.e., sum of entries within each row) of the dropped matrix matches the corresponding row sum of the original.

The heart of the paper discusses the above four smoothed aggregation sub-steps highlighting deficiencies with the standard approach by first examining a simple Poisson operator on a structured mesh that is stretched in one direction. For the first sub-step, we evaluate the use of a distance Laplacian system as an alternative to define the SOC matrix. For the second sub-step we consider algorithms that scale the SOC matrix entries in a non-symmetric fashion. This includes classical AMG [4, 20] as well as some alternatives that we propose such as the *cut-drop* algorithm. For the third sub-step we consider an approach which seeks to find a gap between scaled entries within each matrix row, classifying those on one side of the gap as strong and those on the other side as weak. For the final sub-step, we propose an alternative distributed lumping procedure *distrib-lump* which preserves the row sum without changing the sign of the entries along the matrix diagonal. We compare and contrast the different sub-step algorithms demonstrating the utility of the best-performing algorithms on a set of unstructured test cases, illustrating how the new approaches can avoid some standard SA pitfalls that arise from stretched meshes.

**2. Smoothed Aggregation and its Shortcomings.** In this section, smoothed aggregation AMG is described focusing on the four sub-steps that are intended to address anisotropic phenomena. Before doing this, however, we present a structured stretched model problem that will be used to highlight smoothed aggregation shortcomings by contrasting it with a proper structured geometric multigrid algorithm.

**2.1. Structured Geometric Multigrid Semi-Coarsening.** As noted, mesh coarsening should only occur in directions where relaxation is effective. To illustrate this, consider a Poisson problem

$$(2.1) \quad -\Delta u = g$$

on a cuboid domain  $\Omega$  with Dirichlet conditions on all boundaries except the two  $yz$ -planes, which have Neumann boundary conditions. The discrete linear system

$$(2.2) \quad Au = f$$

is obtained by employing tri-linear hexahedral nodal finite elements on a tensor-product mesh with constant mesh spacing in the  $x$  and  $y$  directions given by  $h$ . The constant mesh spacing in the  $z$  direction is given by  $\alpha h$ .

Consider now a semi-coarsening structured geometric multigrid method,  $\text{SEMI}_{\bar{\alpha}}$ , that always coarsens in the  $x$  and  $y$  directions but only coarsens in the  $z$  direction if the  $z$  mesh spacing is less than or equal to  $\bar{\alpha}$  times the  $x$  spacing on that mesh. Thus,  $\text{SEMI}_{\infty}$  corresponds to standard multigrid that coarsens in all directions. When  $\alpha \gg 1$ , a  $\text{SEMI}_1$  algorithm would initially construct coarse meshes by only coarsening in the  $x$  and  $y$  directions. Should this lead to a coarse mesh where the mesh spacing is identical in all directions, then it would coarsen in all directions to generate additional coarse meshes. When coarsening occurs, we always consider factors of three along each axis (which is a typical SA coarsening rate in one dimension).

Table 1 shows iteration counts Jacobi-smoothed  $\text{SEMI}_{\bar{\alpha}}$  is applied to a  $82 \times 82 \times 82$  problem. The finest mesh spacing in the  $x$  and  $y$  direction is fixed at  $1/81$  and so the computational domain might be more elongated in the  $z$  direction depending on the value of  $\alpha$ . As an example, a  $\text{SEMI}_3$  algorithm applied to a fine mesh with  $\alpha = 9$  would use the following mesh sequence:  $82 \times 82 \times 82$ ,  $28 \times 28 \times 82$ ,  $10 \times 10 \times 28$ , and

TABLE 1

CG iterations ( $10^{-10}$  residual reduction tolerance) with 4 level multigrid V-cycle preconditioner and 1 pre- and 1 post-Jacobi relaxation sweep on all levels, except coarsest which uses a direct solver. The Jacobi damping parameter is .6. Quote marks indicate identical coarsening as previous line.

coarsen algorithm	$\alpha =$	1.	3.	9.	27.	81.
SEMI <sub>1</sub>		17	17	22	23	23
SEMI <sub>3</sub>	"	43	40	30	"	
SEMI <sub>9</sub>	"	"	120	86	44	
SEMI <sub>27</sub>	"	"	"	266	127	
SEMI <sub><math>\infty</math></sub>	"	"	"	"	394	

$4 \times 4 \times 10$ . That is, coarsening in the  $z$  direction only starts on the  $28 \times 28 \times 82$  mesh as at this point the  $z$  direction spacing is three times larger than that of the  $x$  and  $y$  directions. Multigrid interpolation employs tri-linear interpolation, restriction is the transpose of interpolation. It is clear that SEMI<sub>1</sub> is generally the best performing algorithm in terms of iteration counts as it does not coarsen in the  $z$  direction until its mesh spacing is comparable to that of the  $x$  and  $y$  directions. Clearly, full isotropic coarsening (SEMI <sub>$\infty$</sub> ) struggles when the  $z$  direction mesh spacing is large relative to the  $x$  and  $y$  spacing. In this scenario, damped-Jacobi

$$u^{(k+1)} \leftarrow u^{(k)} + \omega D^{-1}(f - Au^{(k)})$$

only smooths errors in the  $x$  and  $y$  directions. Here,  $u^{(k)}$  refers to the approximate solution after  $k$  Jacobi iterations,  $\omega$  is a suitable damping parameter, and  $D$  is the diagonal of  $A$ . We note that in these experiments the cost per iteration (not shown here) is slightly higher when one compares SEMI<sub>1</sub> to SEMI <sub>$\infty$</sub> , but the iteration savings far outweigh this additional cost. Using this as a guide, we can see that an algebraic method when applied to an isotropic diffusion equation should avoid coarsening in directions associated with neighboring grid points that are relatively far from the central point. We now describe smooth aggregation and investigate how it behaves on the above model problem.

**2.2. Smoothed Aggregation.** The first step in applying smoothed aggregation to (2.2) is to coarsen the graph associated with  $A$ . In the simplest case, one can apply an aggregation algorithm directly to the graph of the matrix  $A$  with the goal of assigning vertices to each aggregate,  $\mathcal{A}_k$ , so that the resulting  $\mathcal{A}_k$ 's are disjoint, and approximately the same size. These aggregates are effectively coarse mesh points that will be used to define the next mesh in the multigrid hierarchy. A common approach is to choose a vertex that has not yet been assigned to any aggregate and is not a neighbor of an already created aggregate (i.e., no edge connects this vertex to an already assigned vertex). A new initial aggregate is then formed by grouping this chosen vertex with its neighboring vertices. This process is repeated to continue aggregation until only unassigned vertices remain that have at least one neighbor that is assigned to a created aggregate. Additional heuristics are then applied to either merge unassigned vertices into existing aggregates or create a new aggregate by grouping together a cluster of unassigned vertices [27, 25].

While aggregation might be applied directly to  $A$ , we can mimic semi-coarsening if we remove some of  $A$ 's entries. Suppose that for our example problem an auxiliary

$\tilde{A}$  matrix is defined by removing nonzero  $A_{ij}$  when the  $z$  coordinate of the  $i^{th}$  and  $j^{th}$  mesh points satisfy  $z_i \neq z_j$ . In this case, each aggregate will lie entirely within a single  $xy$ -plane. Thus no coarsening is performed in the  $z$ -direction, corresponding to a coarsening scheme that resembles the advantageous SEMI<sub>1</sub> method when  $\alpha \gg 1$ . Of course, if we do not know that the  $z$  direction corresponds to the distant points, then this must somehow be detected. A traditional smoothed aggregation method will attempt to infer this based on whether scaled matrix entries are above or below a user-supplied threshold  $\theta \in [0, 1]$ . Specifically, smoothed aggregation [26, 27] employs the following criterion for retaining  $A_{ij}$  entries:

$$(2.3) \quad |A_{ij}| \geq \theta \sqrt{A_{ii}A_{jj}}.$$

Following classical AMG, these retained entries are referred to as “strong” while discarded entries are termed “weak”. One advantageous aspect of this criterion is that it is symmetric in nature. That is, if  $A$  is symmetric and  $A_{ij}$  satisfies (2.3), then  $A_{ji}$  must also satisfy (2.3) implying that  $\tilde{A}$  retains  $A$ ’s symmetry property. In contrast to smoothed aggregation, classical AMG [4, 20] employs a different criterion

$$(2.4) \quad -A_{ij} \geq \theta \max_{k \neq i} -A_{ik}.$$

Though this criterion is not symmetric, it does have advantages (discussed shortly) over (2.3). Notice that this criterion drops all positive off-diagonals entries if at least one off-diagonal entry is negative. While this generally works fine for standard discretizations of Poisson operators, it may not be valid for more sophisticated PDEs or for exotic discretizations as it assumes that any positive entry must be weak.

Figure 1 depicts the matrix stencil for an interior grid point as a function of  $\alpha$

$$(2.5) \quad A_{i:} = \begin{cases} \frac{h}{18\alpha} \begin{pmatrix} 1 - 4\alpha^2 & & & \\ & 4 - 4\alpha^2 & & \\ & & 16 + 32\alpha^2 & \\ & 4 - 4\alpha^2 & & \\ & & & 1 - 4\alpha^2 \\ & & 4 - 4\alpha^2 & \\ & & & 1 - 4\alpha^2 \end{pmatrix}, & \text{middle } xy\text{-plane} \\ \frac{h}{18\alpha} \begin{pmatrix} -\frac{1}{2} - \alpha^2 & -2 - \alpha^2 & -\frac{1}{2} - \alpha^2 \\ -2 - \alpha^2 & -8 + 8\alpha^2 & -2 - \alpha^2 \\ -\frac{1}{2} - \alpha^2 & -2 - \alpha^2 & -\frac{1}{2} - \alpha^2 \end{pmatrix}, & \text{top/bottom } xy\text{-plane} \end{cases}$$

FIG. 1. Stencil for  $z$ -stretched example. Identical stencil values are highlighted with identical boxes or ovals (dotted rectangles, solid rectangles, dotted ovals, solid ovals)

for our example  $z$ -stretched mesh (see Appendix B for details). When  $\alpha \gg 1$ , one would hope that off-diagonals corresponding to connections within the middle  $xy$ -plane would be retained (2.3) and that connections between the central mid-plane vertex and a vertex in a different  $xy$ -plane would not. Figure 2 plots the scaled matrix entries  $|A_{ij}|/\sqrt{A_{ii}A_{jj}}$  which must be less than the user-supplied  $\theta$  in order to be dropped. For any  $\theta$  less than approximately .1, the criterion will properly retain all

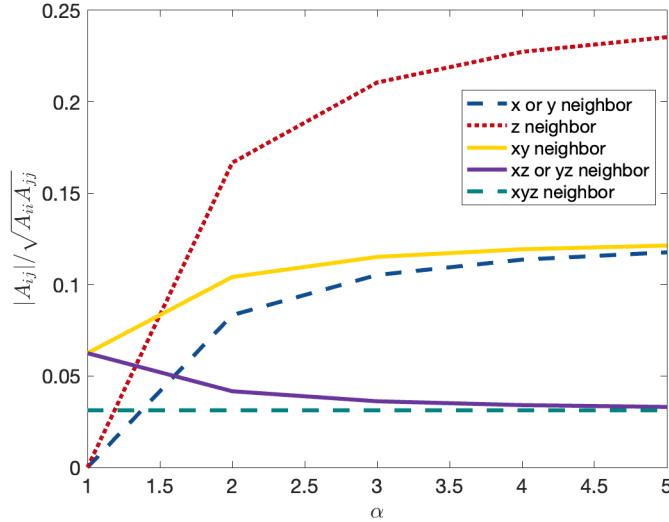


FIG. 2. Traditional SA criterion values for Figure 1 stencil.

of the mid-plane entries (those associated with the blue and yellow lines) for  $\alpha \geq 3$ . Additionally, almost all entries (for the purple and green lines) associated with the top and bottom planes will be discarded for  $\alpha \geq 3$  and  $\theta > .037$ . Unfortunately, however, the dotted oval stencil values (just above and below the central value) give rise to the largest magnitude scaled entries. Thus, the standard smoothed aggregation criterion fails completely on this example as it would not restrict coarsening to just within each  $xy$ -plane even when  $\alpha$  is large. While these failure could be circumvented by always dropping all positive off-diagonal entries, this trick would not necessarily work for other PDEs and other discretizations. In general, we find that basing strong/weak decisions solely on the scaled matrix entries can be unreliable for finite element discretization due in part to a smearing effect related to the inner products between basis functions.

Though somewhat less obvious from the above plot, there are also shortcomings to how matrix entries are scaled with the standard smoothed aggregation criterion. Notice that any  $\theta$  greater than .0625 will discard all off-diagonal entries for  $\alpha = 1$  even though relaxation is effective at removing oscillatory error in all directions. This implies that we would need to choose  $.037 \lesssim \theta \lesssim .0625$  in order to successfully use the same  $\theta$  over a range of different  $\alpha$ . This has implications for finite element applications where the element aspect ratio varies significantly across the mesh, which is quite common in many cases such as when boundary layers are present. Such a limited range of suitable thresholds for such a simple model problem hints at a more problematic concern for more complex applications where users have little intuition about how best to choose this  $\theta$ . While part of this shortcoming is tied to the misleading nature of the matrix coefficients in this case, another part of the difficulty arises from how strength-of-connection entries are scaled. It is worth noting that the classical AMG criterion given by (2.4) always retains at least one negative off-diagonal entry (if present), and so it avoids the pitfall of dropping all off-diagonals entries, which can easily happen with the smoothed aggregation criterion. One highly problematic case for the smoothed aggregation criterion is given in [Appendix A](#) for a 2D version of this same stretching problem where  $\theta$  must be less than .125 to avoid dropping all

off-diagonals in the isotropic case but needs to be greater than .125 to properly semi-coarsen in the anisotropic case<sup>2</sup>. As will be discussed in [subsection 3.2](#), this issue where all off-diagonals are dropped tends to be more likely when the number of nonzeros per row is large (which is common for AMG on coarse grids).

There is one additional smoothed aggregation sub-step that affects behavior for stretched-mesh/anisotropic applications related to the characteristics of the dropped matrix,  $\tilde{A}$ . In smoothed aggregation, a prolongator is constructed in two steps. The first step builds a tentative prolongator  $P_t$  which is effectively a boolean matrix (values of zero or one) for scalar PDE applications. Specifically,

$$(P_t)_{ij} = \begin{cases} 1 & \text{if } i \in \mathcal{A}_j \\ 0 & \text{otherwise} \end{cases}$$

where again the set  $\mathcal{A}_j$  includes the index of all fine level vertices in the  $j^{th}$  aggregate and  $\mathcal{A}_j \cap \mathcal{A}_k = \emptyset$  for all  $j \neq k$ . As the tentative prolongator is not generally optimal in a standard multigrid V cycle<sup>3</sup>, a Jacobi-like prolongator smoothing step is then applied to improve the interpolation operator via

$$(2.6) \quad P = (I - \omega \tilde{D}^{-1} \tilde{A}) P_t$$

where  $\tilde{D}$  is the diagonal of  $\tilde{A}$  and  $\omega$  is a damping parameter that is typically chosen as an inexpensive approximation to  $4/(3\rho(\tilde{D}^{-1} \tilde{A}))$  with  $\rho(K)$  defined as the spectral radius of  $K$ . The dropped matrix must be used in (2.6) so that the number of nonzeros in  $P$  is not large when aggregation is applied to an  $\tilde{A}$  where many dropped entries have been excluded from  $A$ . In particular, using  $A$  in (2.6) could lead to excessive fill-in when constructing the coarse version of the PDE operator via the Galerkin projection  $P^T A P$ . Additionally, the support of each of the prolongator basis function (nonzero pattern within each column) would extend in weak directions if  $A$  is instead used in (2.6), and so interpolation would combine information in oscillatory directions, which we had hoped to avoid.

To maintain smoothed aggregation's optimal convergence properties, it is important that the action of  $\tilde{A}$  applied to a smooth vector should approximately match the action of  $A$  applied to the same smoothed vector, which may not be the case when  $\tilde{A}$  is defined by only zeroing out some entries from  $A$ . Instead, the retained nonzeros must also be modified to at least ensure that

$$(2.7) \quad s \approx \tilde{s} \quad \text{where } s = Av, \quad \tilde{s} = \tilde{A}v, \quad \text{and } v \text{ is a constant vector.}$$

It is worth noting that most entries of  $s$  are typically zero for many discretized PDE matrices, mirroring the fact that differentiation of a constant function is identically zero. To guarantee (2.7), the standard smoothed aggregation procedure [27] defines  $\tilde{A}$  in the following way

$$(2.8) \quad \tilde{A}_{ij} = \begin{cases} A_{ij} & \text{if } i \neq j \text{ and } (i, j) \in \mathcal{S} \\ 0 & \text{if } (i, j) \notin \mathcal{S} \\ A_{ii} + \sum_{(i, k) \notin \mathcal{S}} A_{ij} & \text{if } i = j \end{cases}$$

where  $\mathcal{S}$  is the sparsity pattern that includes all nonzeros of  $A$  that are not dropped. That is, the sum of the dropped entries within each row is lumped to the diagonal entry of that row.

<sup>2</sup>If the trick of discarding all positive off-diagonals is not used, then  $\theta$  must be greater than .25.

<sup>3</sup>Optimal convergence can be achieved with  $P_t$  using special multigrid cycles and small aggregates [17].

While the standard lumping procedure often works fine, we have noticed scenarios where for some  $i$ ,  $\tilde{A}_{ii} < 0$  even though  $A_{ii} > 0$ . Even a single negative diagonal entry can generate a  $P$  (via (2.6)) that is equivalent to or worse than  $P_t$ . Additionally,  $\omega$  might be nonsensical (e.g., negative) due to a negative eigenvalue estimate that again ruins the prolongator smoothing step. Though somewhat contrived, it is possible to illustrate a bad lumping scenario even with our simple stretched example. Specifically, if the dropped entries from the stencil in Figure 1 correspond to those with values  $-\frac{1}{2} - \alpha^2$  (green dotted rectangles),  $-2 - \alpha^2$  (purple ovals), and  $1 - 4\alpha^2$  (yellow rectangles), then it is easy to verify that  $\tilde{A}_{ii} = 0$  using (2.8). Recalling our earlier remarks to “*avoid coarsening in directions associated with neighboring grid points that are relatively far*,” we note that in terms of Euclidean distance from the central point, the vertices associated with the  $-\frac{1}{2} - \alpha^2$  terms are the furthest for  $\alpha > 1$ . The vertices for the  $-2 - \alpha^2$  terms are the second furthest, and the vertices for the  $1 - 4\alpha^2$  terms are the third furthest when  $1 < \alpha < \sqrt{2}$ . Though this failure range is somewhat narrow, it illustrates that a criterion based on distance in conjunction with standard smoothed aggregation lumping could easily lead to problematic diagonal entries for a subset of  $\tilde{A}$ ’s rows. A more realistic example will be shown later in the paper.

**3. Smoothed Aggregation Enhancements.** We consider alternatives to the standard smoothed aggregation process. The first employs a distance Laplacian strength-of-connection (SOC) matrix. The second considers trade-offs between symmetric and non-symmetric scaling algorithms such as (2.4). The third alternative classifies strong and weak connections based on the first *large* gap between scaled SOC entries within a row. The final enhancement defines  $\tilde{A}$  via a new lumping method.

**3.1. SOC matrix.** The strength-of-connection matrix typically coincides with the discretization matrix  $A$ . However, a different auxiliary matrix could have more desirable properties. In addition to the dropping phase, this auxiliary matrix could be used within the prolongator smoothing phase. This might even be necessary for saddle point PDEs if some diagonal entries are identically zero (c.f., [28]). In this case,  $A$  is only used in the Galerkin projection step and not used to construct  $P$ . In this paper, we instead focus on the scenario where dropping decisions are based on the distance Laplacian while a dropped version of  $A$  is used within the prolongator smoother step (see Section 2.2), and so  $P$  is influenced by  $A$ ’s characteristics.

The *distance Laplacian* described in [21] is defined as

$$(3.1) \quad L_{ij} = -\|\mathbf{x}_i - \mathbf{x}_j\|^{-2}, \quad \text{for } A_{ij} \neq 0 \text{ and } i \neq j$$

and  $L_{ii} = -\sum_{i \neq j} L_{ij}$ . Clearly,  $L$  has the following characteristics:

- large (small) magnitude off-diagonal entries correspond to relatively near (far) neighboring mesh vertices from the vertex associated with the diagonal entry;
- same sparsity pattern as  $A$ , and  $L$  is symmetric if the pattern is symmetric;
- negative off-diagonal entries;
- all row sums are zero.

For the model problem, SA coarsening applied to the distance Laplacian should mimic the desired semi-coarsening behavior because off-diagonal entries are the square of inverse distances. Notice that distance Laplacian entries resemble those of a 5-pt (or 7-pt) finite difference Poisson discretization (FD) in two (or three) dimensions on a structured mesh with uniform spacing. In particular, the off-diagonal entries are  $-h_x^{-2}$ ,  $-h_y^{-2}$ , and  $-h_z^{-2}$  in the  $x$ ,  $y$ , and  $z$  directions respectively, where  $h_k$  is the mesh spacing along the  $k^{\text{th}}$  axis. In this way,  $L$  can be viewed as a very crude

approximation to a Poisson operator that avoids finite element (FE) smearing effects. In terms of FE solution accuracy, these smearing effects are addressed by the mass matrix and linear system right hand side, both not normally available to a typical AMG setup procedure.

One disadvantage of the distance Laplacian is that coordinates must be supplied by the application. In our experience, we find that providing coordinates is easy for most application developers. This is in contrast with supplying complete mesh information (e.g., element geometry/connectivity), which is onerous and requires non-trivial code interfaces. Within the AMG implementation,  $L$  can be explicitly formed and projected to coarse levels. Storage can be reduced using a low precision  $L$  and/or retaining only its sparsity pattern once dropping decisions are made. Alternatively, one can implicitly define  $L$  by projecting coordinates to coarser levels, reducing storage further.

A second disadvantage to the distance Laplacian is that important PDE features might be missed when coarsening or when defining  $P$ 's sparsity pattern. For example, if the PDE is anisotropic or if its coefficients include large variations or discontinuities (e.g., due to multiple materials), these features will not influence coarsening. However, if sub-par AMG performance is mainly due to mesh stretching for a particular application, then distance Laplacians are attractive. For some engineering applications, distorted meshes with poor element aspect ratios are the primary source of AMG difficulties. It is important to note that the prolongator still incorporates information from the discretization matrix through  $\tilde{A}$ , albeit not for coarsening decisions.

**3.2. SOC Scaling and Nonsymmetry.** SOC scaling is generally necessary. This can be seen by considering a linear system  $Bu = f_b$  where  $B = \gamma A$  and  $f_b = \gamma f$ . This might occur if the mesh spacing is stretched uniformly in all coordinate directions. We would expect that dropping decisions for  $B$  would be identical to those when solving  $Au = f$ , but scaling must be introduced to preserve this invariance. Scaling effectively defines diagonal matrices  $D_\ell$  and  $D_r$  and considers a scaled SOC matrix

$$(3.2) \quad D_\ell^{-1} S D_r^{-1}.$$

For SA,  $D_\ell = D_r$  and  $(D_r)_{ii} = \sqrt{S_{ii}}$ . For classical AMG,  $D_r = I$  and  $(D_\ell)_{ii} = \max_{k \neq i} -S_{ik}$ . In either case,  $D_\ell$  and  $D_r$  offset the uniform scaling of  $S$  by  $\gamma$ .

Our original preference for the smoothed aggregation criterion has been based on symmetry advantages. Specifically, the graph of the scaled strength-of-connection matrix is represented with undirected edges when it is a symmetric. Recalling the aggregation process, any two vertices in the  $m^{\text{th}}$  aggregate are connected by a path in the strong scaled strength-of-connection graph. When  $D_\ell^{-1} S D_r^{-1}$  is non-symmetric, directed edges are needed. Two vertices in  $\mathcal{A}_m$  should be connected by directed edges in the strong graph, but the path does not necessarily respect strong edge orientations. In fact, the specifics of the aggregate might depend on implementation details. To understand this, consider the 1D mesh in Figure 3 where vertices are

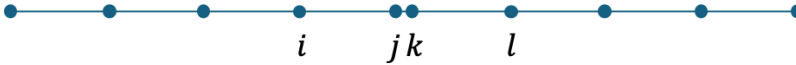


FIG. 3. Mesh with 2 nearby vertices relative to distances between other adjacent vertices.

uniformly spaced except for two vertices that are close together. When  $S = L$ , the

SA criterion determines that edge  $(j, k)$  is strong while edges  $(i, j)$  and  $(k, l)$  are weak if a suitable  $\theta$  is chosen. This means that an aggregate that includes only  $j$  and  $k$  is always formed. With the classical AMG criterion, however, the directed edge  $(i \rightarrow j)$  is strong as  $i$ 's left and right neighbors are equi-distant from  $i$ 's location. Conversely, edge  $(j \rightarrow i)$  is weak as  $j$ 's right neighbor is much closer than its left neighbor. The same sort of split decision occurs for  $(k \rightarrow l)$  and  $(l \rightarrow k)$ . This implies that vertices  $j$  and  $k$  will reside in different aggregates if the aggregation procedure initially chooses the  $i^{th}$  vertex to form one new aggregate (which includes  $j$  and  $i$ 's left neighbor) and the  $l^{th}$  vertex to form another (which includes  $k$  and  $l$ 's right neighbor). Notice that the path from  $j$  to  $i$ 's left neighbor relies on strong edge  $(i \rightarrow j)$ , which has the wrong orientation. If instead vertex  $j$  or  $k$  happens to be chosen as the initial vertex to form an aggregate, then an aggregate that includes only  $j$  and  $k$  is formed as in the SA criterion case. In this sense, a symmetric scaled SOC matrix seems superior in that it always aggregates the nearby  $j$  and  $k$  vertices together regardless of aggregation details.

So what are the disadvantages of the symmetric SA criterion? The biggest disadvantage is that it can frequently determine that all off-diagonal nonzeros should be dropped even when relaxation is effective in all directions. To examine this, consider the case where all of  $S$ 's off-diagonal entries are negative (e.g., using many common finite difference schemes or using a distance Laplacian as the SOC matrix). The sum of entries within a row corresponding to the domain interior is frequently zero. In this case, the SA strong criterion can be re-written as

$$(3.3) \quad \frac{|S_{ij}|}{\sqrt{p_i p_j} \sqrt{|\bar{S}_i \bar{S}_j|}} \geq \theta$$

where  $\bar{S}_k$  is the average of all off-diagonal nonzeros in the  $k^{th}$  row and  $p_k$  is the number of off-diagonal nonzeros in the  $k^{th}$  row and column. When the variance of the off-diagonal values is relatively small (e.g., element aspect ratios close to one),  $S_{ij}/\bar{S}_i \approx 1$  and  $S_{ij}/\bar{S}_j \approx 1$ . This implies that the magnitude of the scaled entries is sensitive to the number of nonzeros within a row/column and that the left hand side of (3.3) becomes small for all off-diagonals when  $\sqrt{p_i p_j}$  is large.

In general, the number of nonzeros per row is higher for 3D domains than for 2D domains. Even on the finest grid, the number of nonzeros per row can also vary noticeably depending on how many elements share a corner vertex. Further, the number of nonzeros per row is often significantly higher and more variable on coarser AMG grids. All of this suggests that a row might contain only weak off-diagonals simply because the number of nonzeros in this row is large. While software checks can be included to prevent division by zero (as the associated diagonal entry of  $\tilde{A}$  must be set to zero to maintain row sums), multigrid convergence and the cost per iteration (due to a lack of coarsening) can still be seriously impacted when this *all-dropping* occurs across many rows. Notice that all-dropping cannot happen with the classical criterion as it is guaranteed to identify at least one off-diagonal in each row as strong (if there is at least one negative entry). Further, it will properly retain most of the entries in the isotropic or low variance case. Thus, the non-symmetric criterion has an important advantage over the SA criterion.

Before concluding this sub-section, we briefly note that any non-symmetric criterion can be modified to form a symmetric criterion. One simple strategy classifies an edge  $(i, j)$  as strong only if the non-symmetric criterion classified either  $(i \rightarrow j)$  or  $(j \rightarrow i)$  as strong. Alternatively, one could only classify edge  $(i, j)$  as weak only if the

non-symmetric criterion classified either  $(i \rightarrow j)$  or  $(j \rightarrow i)$  as weak. Similarly, one could average the scaled entries associated with  $(i \rightarrow j)$  and  $(j \rightarrow i)$  before classification. We do not consider symmetrization further in this manuscript as we have not observed a significant advantage to it on stretched mesh Poisson problems.

**3.3. Classification Based on Gaps.** The scaled SOC entries within a row are often distributed in a clustered fashion with several similar-magnitude values followed by a gap and then additional similar-magnitude values. For example, entries associated with the normal and tangential directions of a boundary layer often lie in distinct clusters. A threshold approach must employ a suitable  $\theta$  to effectively separate clusters. In some cases, it can be challenging to find a  $\theta$  that does this over an entire mesh's rows. The cut-drop algorithm (summarized in Algorithm 3.1) that we now present takes a different approach that directly aims to find a gap between clusters. While we have not described or systematically evaluated it previously, the cut-drop algorithm was incorporated in the MueLu [19] software several years ago. Cut-drop

---

**Algorithm 3.1**  $E_r = \text{CutBasedDropping}(S, \theta_g)$   
*/\*  $S \in \mathbb{R}^n \times \mathbb{R}^n$ : SOC matrix;  $\theta_g$ : gap tolerance;  $E_r$ : retained edges \*/*

---

```

 $E_r \leftarrow \emptyset$ 
/* Define symmetric-scaled values */
 $v_{ij} \leftarrow |S_{ij}| / \sqrt{S_{ii}S_{jj}}$   $\forall i \neq j$  and  $(i, j) \in \mathcal{G}_s$  /*  $\mathcal{G}_s$  is graph of  $S$  */
for  $i = 1, \dots, n$  do
   $(\hat{v}, \hat{j}) \leftarrow \text{descendSort}(v_{i*})$  /*  $\hat{j}_k$  is column index of  $\hat{v}_k$  ( $k^{th}$  largest nonzero). */
   $E_r \leftarrow E_r \cup (i, \hat{j}_1)$ 
   $k \leftarrow 2$ 
  lastEdgeStrong  $\leftarrow \text{true}$ 
  while  $((k \leq \text{length}(\hat{v})) \text{ AND } \text{lastEdgeStrong})$  do
    if  $\hat{v}_k / \hat{v}_{k-1} \geq \theta_g$  then
       $E_r \leftarrow E_r \cup (i, \hat{j}_k)$ 
    else
      lastEdgeStrong  $\leftarrow \text{false}$ 
    end if
     $k \leftarrow k + 1$ 
  end while
end for

```

---

begins by scaling entries symmetrically (like standard SA). Instead of thresholding the scaled  $v_{ij}$  entries, they are sorted within each row. The largest scaled entry within a row is always classified as strong (like the classical criterion). The next largest  $v_{ij}$  within a row is then classified as strong only if the ratio between this  $v_{ij}$  and the previous one is above (or equal to) a tolerance. If this is the case, the process is repeated for the next entry computing a ratio with the most recently classified strong entry. Once an edge is classified as weak, then all remaining smaller scaled entries are classified as weak within the row. Notice that while the scaling is symmetric, classification within each row is independent of other rows, and so the final strong matrix is non-symmetric.

**3.4. Lumping the dropped matrix.** To maintain matrix row sums while also preserving the sign of the diagonal entry, a new lumping procedure is proposed and summarized in Algorithm 3.2. The new algorithm is much simpler than the procedure

---

**Algorithm 3.2**  $\tilde{A} = \text{DropWithLumping}(A, \tilde{\mathcal{S}})$ 


---

*/\* A: undropped matrix;  $\tilde{\mathcal{S}}$ : target sparsity pattern;  $\tilde{A}$ : dropped matrix*


---

*/\* Construct initial dropped matrix  $\tilde{A}$  \*/*
 $\bar{a}_{ij} \leftarrow a_{ij}, \forall (i, j) \in \tilde{\mathcal{S}}$ 
*rowSum  $\leftarrow A\vec{1}$  /\*  $\vec{1}$  is vector with all entries equal to one. \*/*
 $\delta\text{RowSum} \leftarrow \text{rowSum} - A\vec{1}$ 
 $\bar{A}\text{RowAbsSum} \leftarrow |\bar{A}|v$ 
*/\* Update dropped matrix  $\tilde{A}$  \*/*
 $\tilde{a}_{ii} \leftarrow \bar{a}_{ii} + \delta\text{RowSum}_i, \forall (i, i) \in \tilde{\mathcal{S}} \mid \delta\text{RowSum}_i > 0$ 
 $\tilde{a}_{ij} \leftarrow \bar{a}_{ij} + \delta\text{RowSum}_i (|\bar{a}_{ij}| / \bar{A}\text{RowAbsSum}_i), \forall (i, j) \in \tilde{\mathcal{S}} \mid i \neq j \cap \delta\text{RowSum}_i < 0$ 


---

provided in [14] that has the same goals but lacked guarantees concerning the sign of the diagonal entries of the resulting dropped matrix. In addition to this guarantee, we find that the new algorithm works better. The idea is to perform traditional diagonal lumping when it increases the magnitude of the diagonal entry. If traditional diagonal lumping would instead lower the diagonal entry, we instead distribute the lumped quantity over all the retained entries in a manner that is proportional to their magnitude. Recalling that the actual entries of  $\tilde{A}$  are only used during the prolongator smoothing step and that within this step  $\tilde{A}$ 's entries are left scaled by  $\tilde{D}^{-1}$ , we are interested in two properties related to the lumping procedure. The first concerns the sign of the lumped diagonal entry while the second centers on the magnitude of the negative and of the positive entries in the matrix  $\tilde{D}^{-1}\tilde{A}$ .

**THEOREM 3.1.** *Let  $A$  be an  $n \times n$  matrix with sparsity pattern  $\mathcal{S}$ , having positive diagonal entries and non-negative row sums. Consider a matrix  $\tilde{A}$  whose sparsity pattern  $\tilde{\mathcal{S}} \in \mathcal{S}$  whose nonzero entries (i.e.,  $(i, j) \in \tilde{\mathcal{S}}$ ) are given by*

$$(3.4) \quad \tilde{a}_{ij} = \begin{cases} a_{ij} + e_i \frac{|a_{ij}|}{\sum_{k \in \tilde{\mathcal{S}}} |a_{ik}|} & \text{for } e_i < 0 \\ a_{ij} & \text{for } e_i \geq 0 \text{ and } i \neq j \\ a_{ij} + e_i & \text{for } e_i \geq 0 \text{ and } i = j \end{cases}$$

where

$$(3.5) \quad e_i = \sum_{k \mid (i, k) \in \mathcal{S} \setminus \tilde{\mathcal{S}}} a_{ik}.$$

That is,  $e_i$  is the sum of nonzero entries in  $A$  excluded from the  $i^{\text{th}}$  row of  $\tilde{A}$ . Additionally, assume that for any row  $i$ , there exists at least one  $(i, k) \in \tilde{\mathcal{S}}$  such that  $k \neq i$  and  $a_{ik} < 0$  (at least one negative off-diagonal entry in each row of  $A$  is retained in  $\tilde{A}$ ). Then, the following two properties hold:

- For all  $(i, j) \in \tilde{\mathcal{S}}$ ,  $\text{sgn}(a_{ij}) = \text{sgn}(\tilde{a}_{ij})$  (Entries retain their sign).
- For all  $i$ ,  $\sum_j a_{ij} = \sum_j \tilde{a}_{ij}$  (Identical row sums).

*Proof.* We consider first the case where  $e_i \geq 0$ . As this approach shifts positive values to the diagonal, all signs are preserved as is the row sum. This corresponds to a traditional lumping procedure that does not alter the retained off-diagonal values and modifies the diagonal to maintain the row sums.

Now we consider the  $e_i < 0$  case. We first observe that we can rewrite the

expression for  $\tilde{a}_{ij}$  as

$$(3.6) \quad \begin{aligned} \tilde{a}_{ij} &= a_{ij} \left( 1 + \frac{e_i}{\sum_{k \in \tilde{\mathcal{S}}_i} |a_{ik}|} \right) && \text{where } a_{ij} > 0 \\ \tilde{a}_{ij} &= a_{ij} \left( 1 - \frac{e_i}{\sum_{k \in \tilde{\mathcal{S}}_i} |a_{ik}|} \right) && \text{where } a_{ij} < 0. \end{aligned}$$

The parenthesized expressions in (3.6) include only the sums of excluded or retained entries (or their absolute values), and so these scaling factors are the same for each entry with that particular sign within a given row  $i$ . For  $a_{ij} < 0$ , we have  $e_i < 0$  and a positive denominator, making the parenthesized expression positive so the the first property holds.

For the  $a_{ij} > 0$  case, we define

$$(3.7) \quad r_i^{(p)} = \sum_{j \mid (i,j) \in \tilde{\mathcal{S}} \text{ and } a_{ij} > 0} a_{ij} \quad (\text{sum of positive retained entries}),$$

$$(3.8) \quad r_i^{(n)} = \sum_{j \mid (i,j) \in \tilde{\mathcal{S}} \text{ and } a_{ij} < 0} a_{ij} \quad (\text{sum of negative retained entries}),$$

$$(3.9) \quad s_i = e_i + r_i^{(p)} + r_i^{(n)} \quad (\text{row sum}),$$

for each row where  $e_i < 0$ . We note that  $s_i = \sum_j a_{ij}$ , the sum of  $A$ 's entries in the  $i^{th}$  row. We can now rewrite (3.6) as

$$(3.10) \quad \tilde{a}_{ij} = a_{ij} \left( 1 + \frac{e_i}{r_i^{(p)} - r_i^{(n)}} \right),$$

for all positive  $a_{ij}$ , which obviously includes the diagonal entry. For the third property to hold, we need

$$(3.11) \quad 1 + \frac{e_i}{r_i^{(p)} - r_i^{(n)}} > 0$$

or equivalently that

$$(3.12) \quad e_i + r_i^{(p)} - r_i^{(n)} > 0$$

as the denominator in (3.11) is always positive. Substituting (3.9) for  $e_i$ , into (3.12) the condition becomes

$$(3.13) \quad s_i - 2r_i^{(n)} > 0.$$

We note that  $r_i^{(n)} < 0$  because we assumed that at least one negative off-diagonal is retained. Since  $s_i$  is non-negative, it follows that all positive retained entries (including the diagonal entry) remain positive, and the first property holds.

For the second property in the  $e_i < 0$  case, the row sum of the  $i^{th}$  row of  $\tilde{A}$  is obtained by adding all entries in the top line of (3.4) and corresponds to

$$r_i^{(p)} + r_i^{(n)} + e_i \frac{\sum_{k \in \tilde{\mathcal{S}}} |a_{ik}|}{\sum_{k \in \tilde{\mathcal{S}}} |a_{ik}|}.$$

As this is just the definition of  $s_i$ , we have shown that  $\tilde{A}$  has the same row sums as those of  $A$ , completing the proof.  $\square$

*Remark 3.2.* Notice that if  $s_i = 0$  and no negative entries are retained, then any lumping strategy that maintains row sums must lead to a diagonal entry that is either identically zero or negative. This highlights the importance of keeping at least one negative off-diagonal value. Further notice that should a row have a negative sum (perhaps due to a somewhat atypical boundary condition), then it is still possible that the diagonal remains positive if the sum of the retained negative entries is large enough. Should (3.13) not hold (and so the sign of the diagonal entry changes), we note that traditional lumping would also change the sign of the diagonal as it adds a larger magnitude negative value to the diagonal than the top expression in (3.4). Finally, we note that additional strategies could be considered for rows with negative row sums (e.g., lumping only to off-diagonal negative entries), but we have not experimented with this as we have not encountered a situation where (3.13) does not hold in our experiments.

**COROLLARY 3.3.** *For rows where  $e_i < 0$ , the positive entries of  $D^{-1}A$  are identical to those of  $\tilde{D}^{-1}\tilde{A}$  when (3.4) is used to define  $\tilde{A}$  and the same assumptions in Theorem 3.1 hold. Likewise for rows where  $e_i < 0$ , the negative entries of  $\tilde{D}^{-1}\tilde{A}$  are obtained by scaling the negative retained entries of  $D^{-1}A$  by the factor*

$$(3.14) \quad \frac{1 - \frac{e_i}{\sum_{k \in \tilde{\mathcal{S}}_i} |a_{ik}|}}{1 + \frac{e_i}{\sum_{k \in \tilde{\mathcal{S}}_i} |a_{ik}|}}$$

which is greater than one.

*Proof.* From the proof of Theorem 3.1, we established that all positive entries within a row are scaled by the same factor given by the upper expression between parenthesis of (3.6) and hence all positive entries of  $D^{-1}A$  and  $\tilde{D}^{-1}\tilde{A}$  must coincide when  $e_i < 0$ . We also established in the Theorem 3.1 proof that all negative entries within a row are scaled by the lower expression between parenthesis in (3.6), and so (3.14) follows. Additionally, the denominator is positive and must be smaller than the numerator as  $e_i < 0$ . Thus, the scaling factor must be greater than one.  $\square$

*Remark 3.4.* While it is not completely clear what properties are best for an ideal lumping procedure, we find it natural that the only difference between  $D^{-1}A$  and  $\tilde{D}^{-1}\tilde{A}$  for rows where  $e_i < 0$  is that the constant scaling of the negative entries is a bit larger than the positive entries (which are not scaled) as this larger scaling can be viewed as a way to compensate for the fact that more negative information has been dropped from the stencil, which is reflected by the sum of the excluded entries being negative. Specifically, it can be easily shown that the scaling factor for negative entries when  $s_i = 0$  (i.e., interior rows) and  $e_i < 0$  is given by  $r_i^{(p)} / |r_i^{(n)}|$ . That is, the scaling factor only becomes large to compensate for the case when most negative entries have been dropped.

*Remark 3.5.* While preserving the sign of the diagonal entries, the lumping procedure described in Theorem 3.1 does not maintain the symmetry of  $A$  nor does it guarantee that  $\tilde{A}$  has all positive eigenvalues (which is also not guaranteed by traditional diagonal lumping). While this can cause degradation in the quality of the prolongator smoothing step, we find it far less harmful than when even a single diagonal entry changes sign.

**4. Computational Examples.** A variety of stretched mesh examples are considered to assess different sub-stage classification methods. All examples employ an

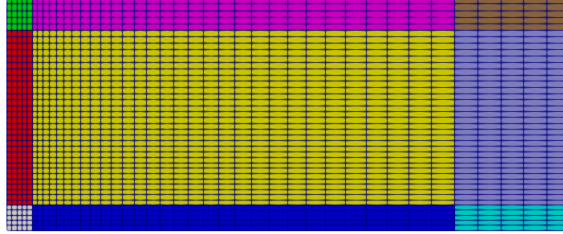


FIG. 4.  $2x$  de-refinement of 2D tensor-product mesh with stretch factors of  $\gamma_1 = 4.5459$  and  $\gamma_2 = 1.2877$ .

algebraic multigrid preconditioner through the MueLu [19] software package. MueLu is set to generate multigrid levels until the coarse problem is under 1,000 unknowns. A multigrid V cycle is used with 1 pre- and 1 post- symmetric Gauss-Seidel iteration on all tests. For all examples, linear finite elements using either quadrilateral, triangular (only for the cavity mesh) or hexahedral elements are employed to discretize a Poisson operator. When solving the associated linear systems, the right hand side is chosen (for all but the cavity problem) so that the 2D solution is  $u(x, y) = 1 + x + y + xy$ , the 3D solution is  $u(x, y, z) = 1 + x + y + z + xy + xz + yz + xyz$ , and the initial guess satisfies Dirichlet boundary conditions, but is zero elsewhere.

Meshes for the examples described in the first three sub-sections are generated using Pamgen [12]. Appendices C.1-C.3 provide the relevant input decks. Meshes in Section 4.4 are generated using Cubit [1] in conjunction with post-processing to add boundary layers. Finally, the Section 4.5 meshes were generated by different application teams at Sandia.

**4.1. 2D Tensor-Product Stretched Poisson.** A mesh with nine regions is shown in Figure 4. It has an isotropic bottom-left region, a uniformly stretched top-right region, and graded regions in between. Twenty different stretch factors ( $\gamma_1$  and  $\gamma_2$ ) logarithmically spaced between 0.5 and 200 for each dimension are investigated. We only consider meshes where the  $y$ -stretching is greater than or equal to that of the  $x$  stretching, leading to 210 total problems. Dirichlet conditions are applied on the bottom boundary while all other boundaries have Neumann conditions.

Figure 5 shows results for five algorithm combinations using an AMG-preconditioned conjugate gradient (CG) solver, stopping when the residual is reduced by 10 orders of magnitude. Each algorithm is denoted by a name of the form SOC matrix/scaling scheme/classification scheme. The SOC matrix could be either A or DLap to indicate use of the matrix  $A$  or the distance Laplacian respectively. The scaling algorithm could be either SA or Sgn to indicate use of the SA symmetric scaling scheme or the signed classical AMG scheme respectively. The classification algorithm could be either Val or Gap to indicate that classification is based on scaled SOC entry values or gaps (i.e., cut-drop algorithm). These results all employ a traditional diagonal lumping scheme. Each dot corresponds to a single example and measures the overall cost defined as the number of iterations multiplied by operator complexity. The AMG operator complexity is the ratio between the sum of the number of nonzeros in the matrix  $A$  on all levels divided by the number of  $A$ 's nonzeros on the finest level. Blue is the best (cost = 10) and red is the worst (cost = 60). To better distinguish between successful runs, we clip colors at 60. That is, all runs with cost greater than 60 also appear as red dots. A missing dot indicates that either AMG did not converge or

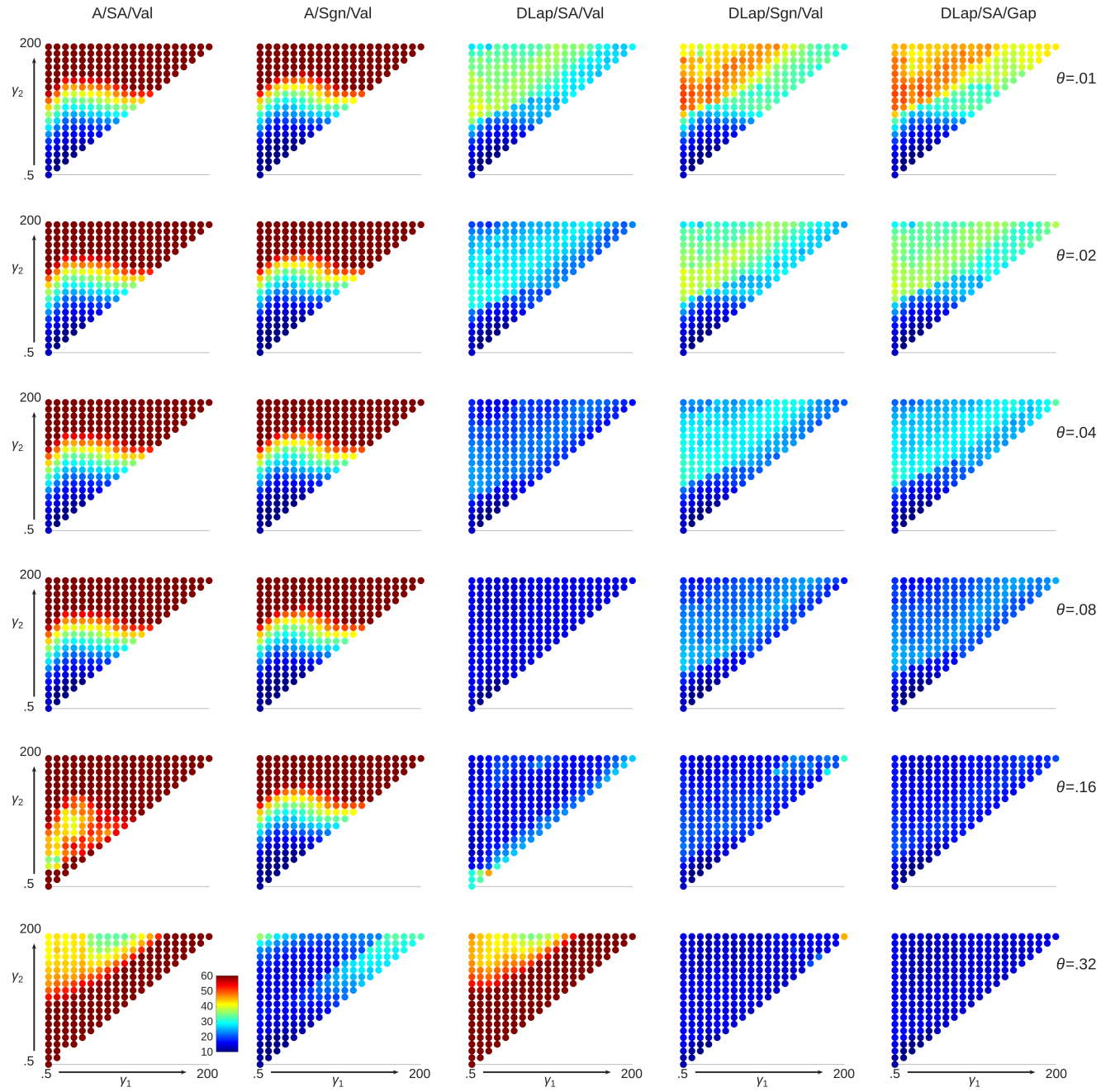


FIG. 5. Iterations  $\times$  operator complexity, with the color scale from 10 to 60 for the 2D mesh. Columns represent algorithm choices (described in Section 4.1) and rows represent tolerances,  $\theta$ . Diagonal lumping is use for all experiments.

the setup procedure broke down (e.g., all off-diagonal entries dropped). In general, it is clear that the distance Laplacian SOC matrix is advantageous when compared to using the  $A$  matrix as the solver converges well over a wide range of  $\theta$ 's. However, A/Sgn/Val for  $\theta = .32$  also performs well. Here, the automatic classification of positive off-diagonals as weak plays an important role. It is interesting to note that A/Sgn/Val, DLap/Sgn/Val, Dlap/SA/Gap all do well with  $\theta = 0.32$ . This  $\theta$  value is much larger than standard AMG recommended choices which tend to be closer to 0.1 or smaller. We will see this trend continue in the examples that follow. We have even observed higher tolerances (e.g.,  $\theta = .64$ ) performing well, though larger  $\theta$ 's give rise to high AMG operator complexities. We note that the operator complexities (not shown separately in the figure) range from 1.11 to 1.44 for  $\theta = .32$  with all three of these algorithm scenarios. As smoothed aggregation AMG normally has very low complexities (e.g., near 1.1 or lower) when compared to classical AMG, it is often possible to more aggressively classify off-diagonals as weak (than might be typical for classical AMG) and still end up with a practical method.

Overall, the two rightmost columns (signed classical AMG scaling with traditional classification versus symmetric SA scaling with cut-drop) are the best methods and perform fairly similarly with cut-drop being slightly better. In particular, there are a few interspersed lighter blue colors and one orange dot with signed classical AMG scaling for larger  $\theta$ 's. The interspersed colors and distributed lumping are discussed more in Section 4.2. Finally, we note that standard SA scaling and classification with the distance Laplacian (the middle column) does fairly well performing best for  $\theta = .08$ . Results for distributed lumping can be found in appendix Figure 15.

**4.2. 3D Tensor-Product Stretched Poisson.** 3D meshes are generated in a similar fashion to the Section 4.1 example except for the addition of a fixed  $z$  dimension containing 80 cells. That is, twenty logarithmically spaced stretch factors between 0.5 and 200 are investigated for the  $x$  and  $y$  dimensions. Dirichlet conditions are applied on the  $y = 0$  boundary while Neumann conditions are applied on other boundaries. CG is again employed, stopping when the residual is reduced by 10 orders of magnitude. Figure 6 shows traditional diagonal lumped results. Generally, it can be seen that the distance Laplacian algorithms tend to perform better over a range of  $\theta$ 's. DLap/Sgn/Val works well over the largest range of  $\theta$ 's while the best individual case occurs for Dlap/SA/Gap with  $\theta = .32$ .

Figure 7 shows the same scenarios using distributed lumping. Here we can see that distributed lumping often modestly improves results. In general, the biggest impact occurs when a diagonal entry in the dropped matrix became negative due to the traditional lumping procedure (which happens more frequently at higher thresholds). Overall, the biggest improvement is seen for DLap/Sgn/Val which is clearly the best performing combination. The method now performs well for  $\theta = .08, .16$ , and  $.32$ . These were also good  $\theta$  choices for the 2D examples, where distributed lumping (see appendix Figure 15) also removes the speckled dots seen in Figure 5 for DLap/Sgn/Val. The DLap/SA/Val results are also noticeably improved for  $\theta = .02$  and  $.08$ . Notice that the best  $\theta$ 's for DLap/SA/Val are now somewhat smaller than for the 2D problem. In general, we find guessing an appropriate  $\theta$  choice for DLap/SA/Val can be challenging compared with choosing  $\theta$  for DLap/Sgn/Val or DLap/SA/Gap. Finally, we note that distributed lumping is not guaranteed to improve AMG convergence. We see that in many cases, the distributed lumping and diagonal lumping give similar results. This can occur when standard lumping is not problematic (i.e., it does not reduce diagonal entries by *too much*) or when convergence limitations are due to sub-optimal

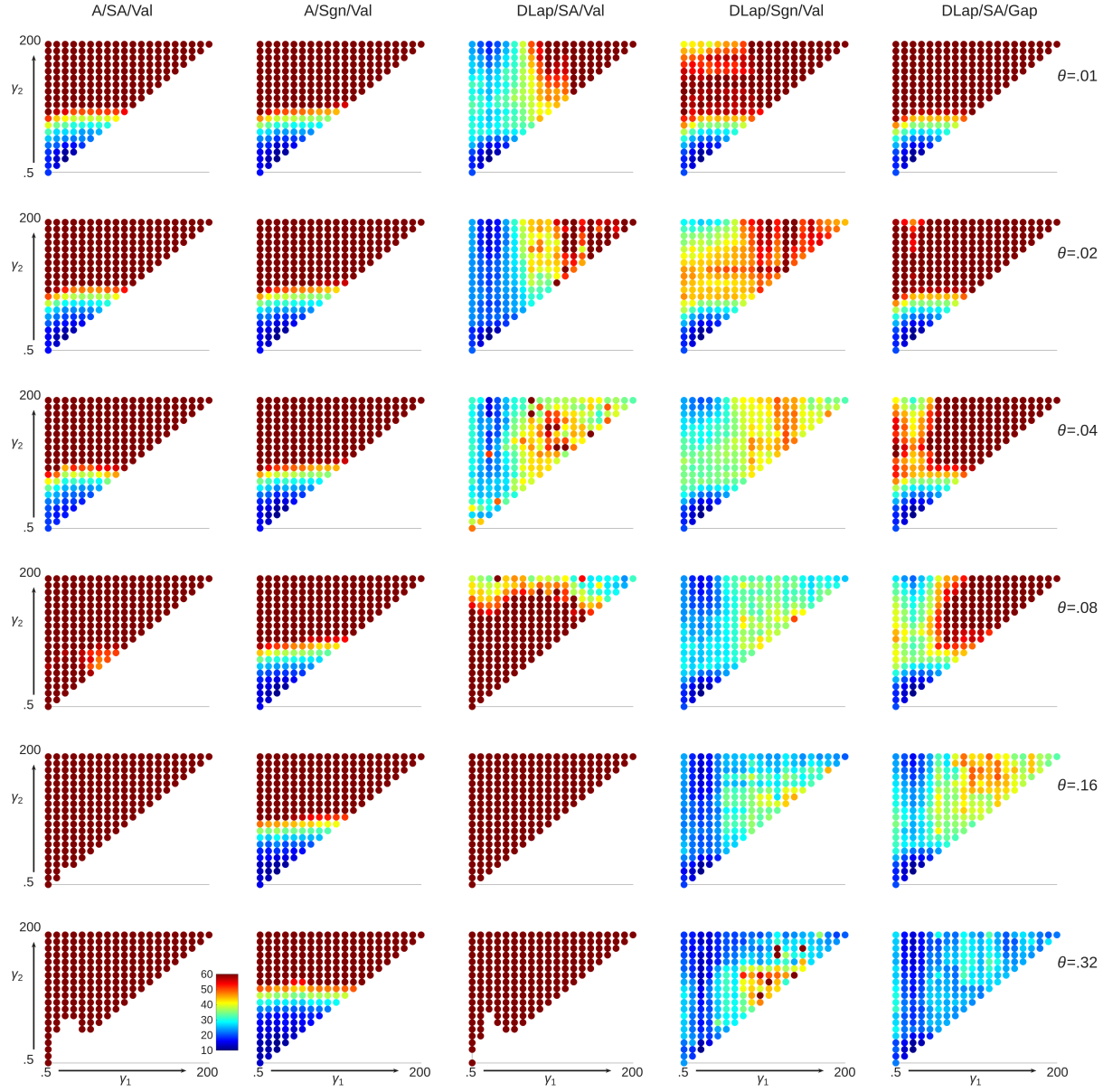


FIG. 6. Iterations  $\times$  operator complexity, with the color scale from 10 to 60 for the 3D mesh. Columns represent algorithm choices (described in Section 4.1) and rows represent tolerances,  $\theta$ . Diagonal lumping is use for all experiments.

classification choices so that changes to the lumping procedure are not impactful. This later case occurs in many of the sub-plots with a large number of red dots. As one can see, there are also situations where standard lumping might perform better. In several of these cases, we've observed that standard lumping produces a negative diagonal entry leading to a large negative eigenvalue estimate. This in turn results in a very small magnitude (and negative) prolongator smoothing damping parameter  $\omega$ .

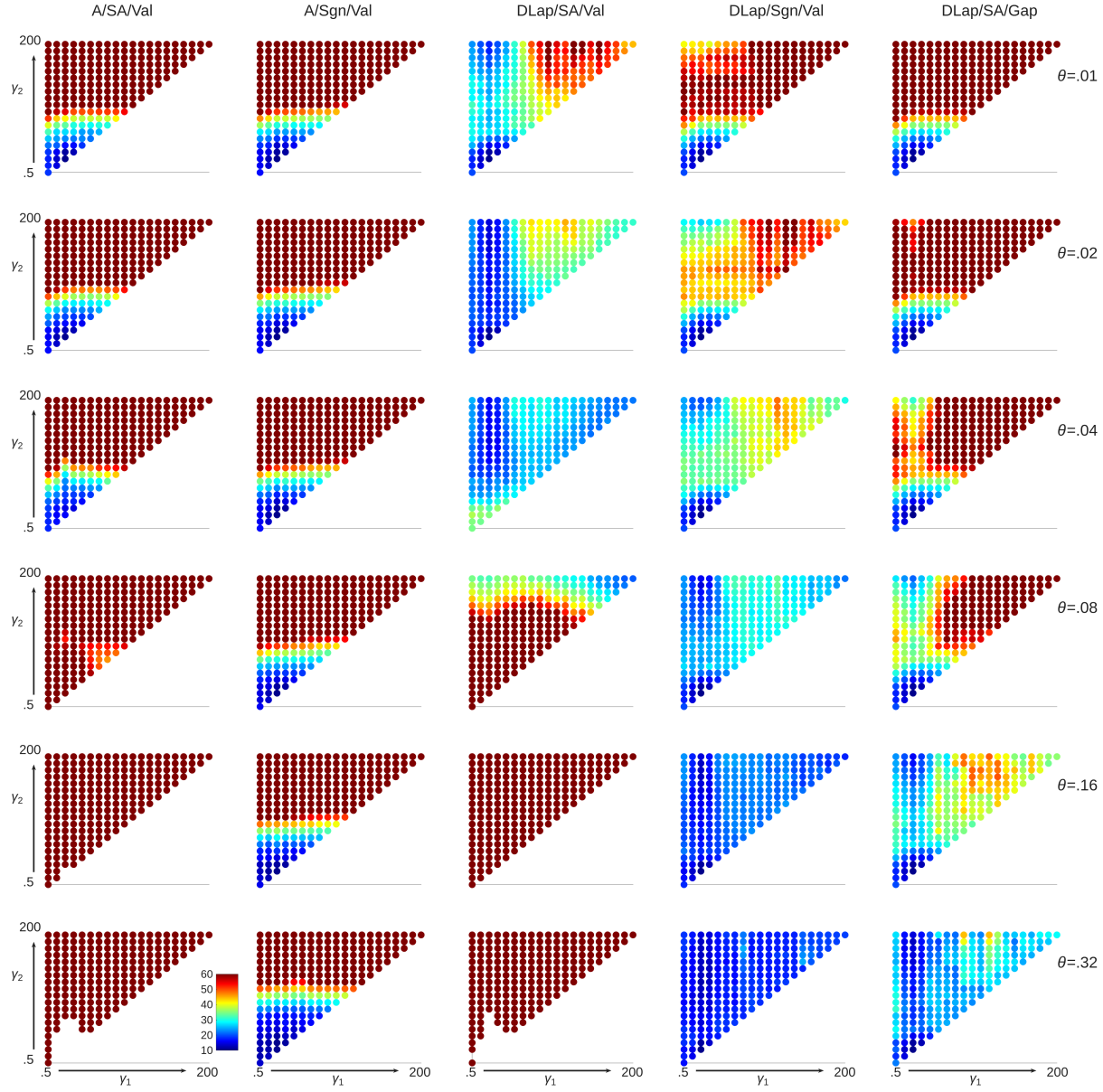


FIG. 7. Iterations  $\times$  operator complexity, with the color scale from 10 to 60 for the 2D mesh. Columns represent algorithm choices (described in Section 4.2) and rows represent tolerances,  $\theta$ . Distributed lumping is use for all experiments.

in (2.6), which oddly enough can have a fortunate beneficial effect. In particular, the resulting grid transfer operator resembles piecewise-constant interpolation. While this interpolation is sub-optimal (when compared to smoothed grid transfer functions), it may actually be better than that obtained with large  $\omega$  prolongator smoothing if the the coarse discretization operator is flawed due to earlier poor classification choices. The DLap/SA/Gap with  $\theta = .32$  case is where some of the distributed lumping results

seem a bit inferior. We have noticed that with large thresholds on coarser grids (where some fill-in has occurred), DLap/SA/Gap might classify many small scaled SOC matrix entries as strong when there is not a nice gap in the magnitude of values within some rows.

**4.3. 3D Radial Trisection Stretched Poisson.** For some applications is not uncommon to pair a radial mesh with a less structured mesh near the origin to avoid degenerate elements, as in (e.g., Figure 8). We vary these innermost-region transition blocks, which we call *trisection blocks*, with values 1, 2, 3, 4 and 6. Depending on

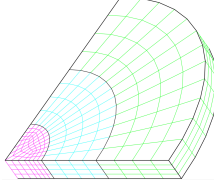


FIG. 8. Sample radial trisection mesh.

the number of trisections, we start by stretching the radial region by a factor of 1.0658 to 1.6426 and increase stretching logarithmically up to 100 leading to 205 cases. Dirichlet conditions are applied on the outer radius while other boundaries have Neumann conditions.

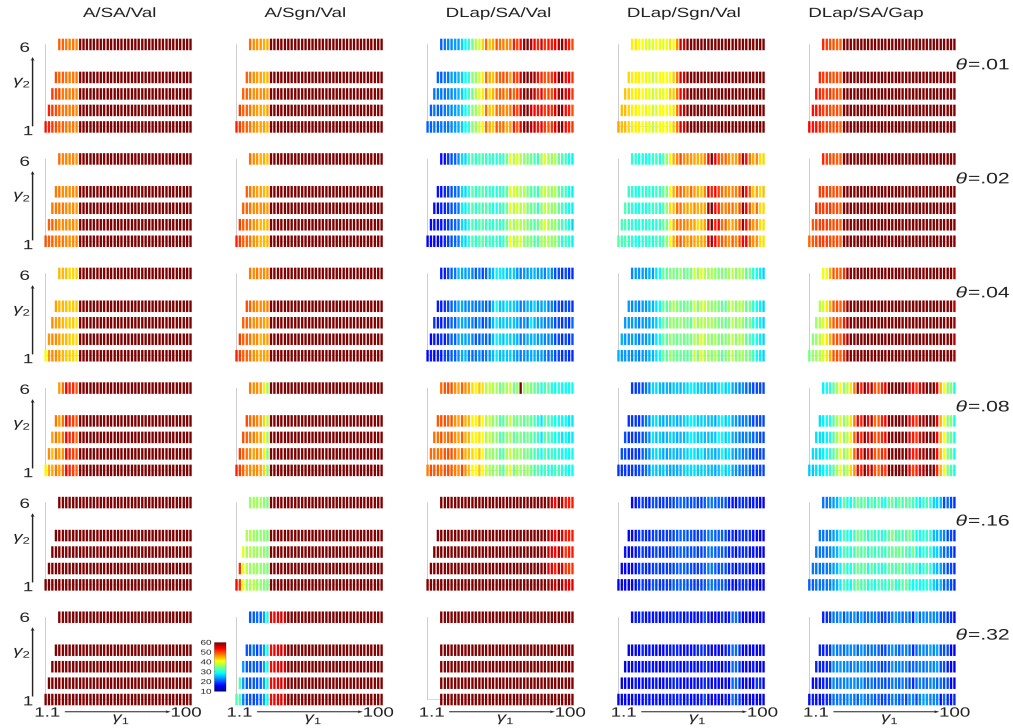
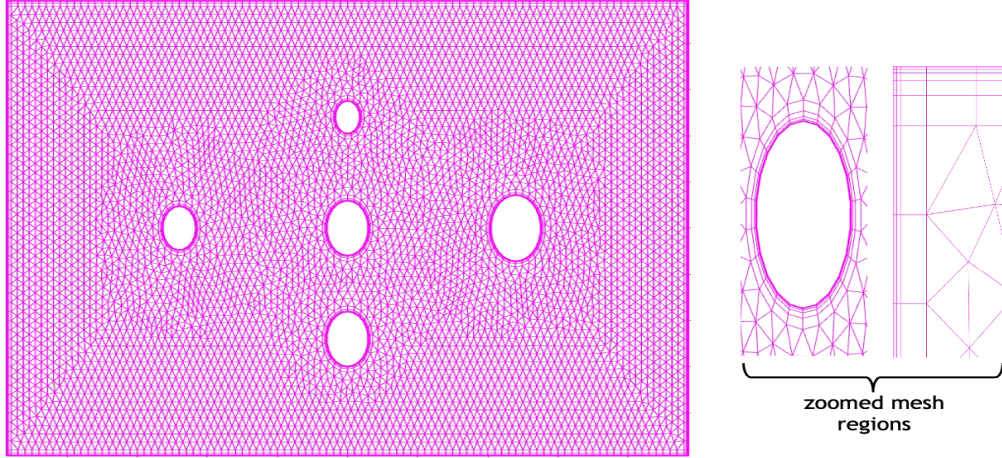


FIG. 9. Iterations  $\times$  operator complexity (distributed lumping) for radial hexahedron case.

Figure 9 shows CG results with distributed lumping where now each run is plotted as a vertical bar. Convergence is declared when the residual is reduced by 10 orders of magnitude. The number of trisection blocks  $\gamma_2$  takes on the values of 1, 2, 3, 4, and 6 (the gap between the top and second line in the sub-figures is due to the

FIG. 10. *Five cavity mesh.*

omission of  $\gamma_2 = 5$ ). These results are fairly consistent with those from the 3D tensor mesh example. We again see that the distance Laplacian methods outperform those that use  $A$  for the SOC matrix. Traditional SA (A/SA/Val in column 1) is the worst. Classical AMG scaling (column 2) improves the situation, but relies heavily on automatically discarding all positive off-diagonals. Among distance Laplacian versions DLap/Sgn/Val (column 4) is the best followed by DLap/SA/GAP (column 5) and then DLap/SA/Val (column 3).

**4.4. 2D Boundary Layer Meshes with Circular Cavities .** We now consider a mesh with circular cavities and includes boundary layers (Figure 10). Dirichlet boundary conditions are present on the top and bottom domain boundaries as well as on the central cavity boundary. The top Dirichlet condition enforces the solution to be one while the other Dirichlet boundaries enforce a zero solution. All other boundary conditions are homogeneous Neumann. Triangular elements are used for non-boundary layer portions of the mesh while quadrilateral elements are used for the boundary layers. The CG algorithm is used with a relative residual tolerance of  $10^{-10}$ . The only nonzero right hand side entries correspond to the top Dirichlet boundary. Table 2 gives the results. A dash entry indicates that the solver did not converge

$\theta$	A/SA/Val			A/Sng/Val			DLap/SA/Val			DLap/Sng/Val			SLap/SA/Gap		
	SL	DL	$\alpha$	SL	DL	$\alpha$	SL	DL	$\alpha$	SL	DL	$\alpha$	SL	DL	$\alpha$
.01	89	88	1.06	73	73	1.07	22	17	1.07	27	25	1.08	32	32	1.08
.01	90	90	1.11	80	80	1.29	36	36	1.17	50	49	1.17	54	54	1.17
.02	92	92	1.11	80	80	1.29	33	33	1.16	45	45	1.16	50	50	1.18
.04	88	88	1.11	80	80	1.29	23	23	1.20	41	41	1.18	45	45	1.16
.08	81	81	1.16	79	79	1.29	31	31	1.36	40	40	1.18	45	45	1.17
.16	94	93	1.35	72	72	1.31	75	75	1.40	35	35	1.18	44	44	1.17
.32	-	-		34	34	1.37	-	-		24	24	1.28	32	32	1.32

TABLE 2

*Iteration counts for standard lumping SL and distributed lumping DL and AMG operator complexities  $\alpha$  for five cavity mesh.*

within 200 iterations. These results mirror those of the previous problems. In par-

ticular, the distance Laplacian variants generally perform better with **DLap/Sng/Val** being the best while **DLap/SA/Gap** is the second best. For the cavity problem, there is no significant difference between using standard and distributed lumping.

**4.5. Meshes from Applications.** We begin this sub-section with a cylinder mesh (left side of Figure 11) that has been used as a simple benchmark for more sophisticated helium plume meshes and studies [24]. All results in this sub-section

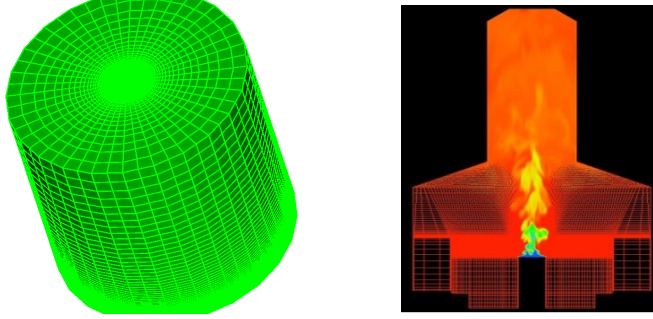


FIG. 11. Partially zoomed image of simplified mesh used for Table 3 (left) and mesh densities with gas density contours overlaid for actual helium plume studies (right).

investigate Poisson problems on stretched meshes that are discretized using linear first order hexahedral finite elements. In all of these examples, Neumann boundary conditions are applied on all but one surface which instead has Dirichlet boundary conditions. For the cylinder mesh, the Dirichlet boundary condition coincides with one of the circular surfaces and the matrix  $A$  has size  $772,585 \times 772,585$ . To limit the required computations needed for the generally larger and more complex meshes in this sub-section, we now employ AMG preconditioned GMRES(300) and convergence is declared when the two-norm of the initial residual is reduced by  $10^{-6}$ . This change was primarily motivated by our last example, which needed to be run in serial due to some mesh partitioning and format conversion limitations.

Table 3 gives iteration counts and AMG operator complexities. The AMG op-

$\theta$	A/SA/Val			A/Sng/Val			DLap/SA/Val			DLap/Sng/Val			SLap/SA/Gap		
	SL	DL	$\alpha$	SL	DL	$\alpha$	SL	DL	$\alpha$	SL	DL	$\alpha$	SL	DL	$\alpha$
.01	89	88	1.06	73	73	1.07	22	17	1.07	27	25	1.08	32	32	1.08
.02	89	86	1.05	74	73	1.07	19	14	1.11	21	21	1.06	29	28	1.09
.04	75	74	1.08	73	74	1.07	31	18	1.22	21	16	1.08	30	30	1.06
.08	71	65	1.17	58	58	1.10	42	39	1.32	20	15	1.11	24	24	1.08
.16	169	105	1.24	58	58	1.13	86	83	1.19	23	12	1.18	18	18	1.13
.32	126	133	1.11	47	46	1.24	138	134	1.06	21	10	1.27	14	13	1.20

TABLE 3

Iteration counts and AMG operator complexities  $\alpha$  for standard lumping  $SL$  and distributed lumping  $DL$  on cylinder mesh problem.

erator complexities for standard and distributed lumping differ by at most .01. To reduce clutter, only the largest of these two complexities is shown for each dropping algorithm/ $\theta$  choice in all tables within this sub-section. For all runs, the number of AMG levels varies between 3 and 5.

From the results, it is clear that variants employing the distance Laplacian SOC matrix are generally better than those that employ  $A$  as SOC matrix. The overall best method is **DLap/Sgn/Val** in that it successfully solves the problem in under 20

iterations with distributed lumping over a wide range of  $\theta$  values. We can also see that distributed lumping generally either reduces the iteration count or has the same iteration count as standard diagonal lumping. There are, however, two non-failure cases where distributed lumping increases the iterations. In one case, one additional iteration is taken while in another case iterations increase from 126 to 133. We typically find that this type of modest increase might occur for poorly converging situations. In one case, distributed lumping reduced the iteration count from 169 to 105 and distribution lumping requires about half as many iterations as standard lumping for the best performing combination: DLap/Sgn/Val with  $\theta \geq .16$ . Finally, we note that for realistic helium plume simulations depicted on the right side of Figure 11, a sophisticated control volume discretization technique is instead employed and the solution evolution requires repeated Poisson solves in a pressure-projection type of method.

We next consider a mesh that is normally used to simulate a jet of fluid perpendicularly entering a cross flow in NALU [23], requiring refined meshes where the jet and cross flow meet to resolve the complex interactions. Figure 12 illustrates a highly zoomed portion of the mesh which essentially corresponds to a small inlet region that

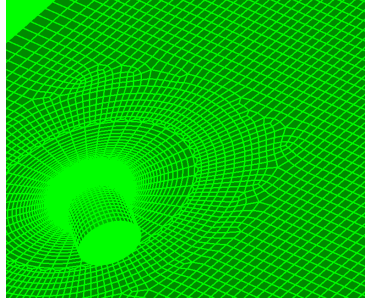


FIG. 12. *Zoomed image of mesh used for Table 4 focusing on inlet where jet enters cross flow.*

is connected to a much larger box near one of its corners. The discrete matrix  $A$  is  $3,548,688 \times 3,548,688$  and the one Dirichlet surface coincides with the circular face at the tip of the inlet. Table 4 gives the iteration counts and AMG operator complexities. A dash indicates that a particular run did not converge within 500 iterations.

$\theta$	A/SA/Val			A/Sng/Val			DLap/SA/Val			DLap/Sng/Val			SLap/SA/Gap		
	SL	DL	$\alpha$	SL	DL	$\alpha$	SL	DL	$\alpha$	SL	DL	$\alpha$	SL	DL	$\alpha$
.01	316	326	1.04	306	314	1.05	27	22	1.21	62	33	1.16	85	88	1.15
.02	313	327	1.04	307	317	1.06	79	32	1.27	45	28	1.19	56	56	1.18
.04	318	302	1.10	307	313	1.06	98	40	1.39	50	24	1.23	38	41	1.22
.08	388	375	1.19	280	283	1.12	113	79	1.48	48	19	1.29	30	30	1.26
.16	-	492	1.32	268	273	1.16	148	146	1.36	45	13	1.35	25	24	1.32
.32	470	432	1.28	266	273	1.35	244	241	1.22	62	10	1.42	16	15	1.37

TABLE 4

*Iteration counts and AMG operator complexities  $\alpha$  for standard lumping SL and distributed lumping DL on inlet jet problem.*

We see that using  $A$  as the SOC matrix generally leads to very poor convergence. In particular, all runs require over 250 iterations. For these poorly converging cases, we can also see a few more situations where distributed lumping might increase the number of required iterations (e.g., from 313 to 327).

The results for the jet inlet problem mirror those of the cylinder mesh, though

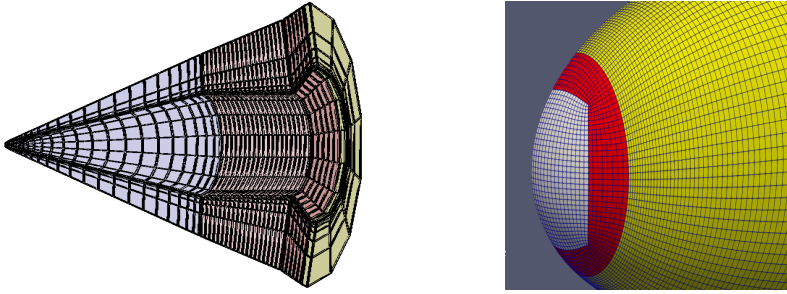


FIG. 13. Left: 6 block coarse version of HIFiRE-1 mesh. Each color denotes a different block structured mesh region. Right: Zoom of outer HIFiRE-1 mesh surface near nose.

more dramatically. In particular, it is possible to solve this problem in under 20 iterations (e.g., with DLap/Sgn/Val and  $\theta \geq .08$ ) while the runs that use  $A$  as opposed to the distance Laplacian require hundreds of iterations. While the distributed lumping DLap/SA/Val runs are somewhat competitive, it is clearly the worst distance Laplacian based method. Similar to the 3D stretched tensor meshes, we find that DLap/SA/Gap generally performs better than DLap/Sgn/Val with standard lumping, but the opposite is true once distributed lumping is introduced. That is, distributed lumping appears to have a more positive impact on the distance Laplacian signed classical scaling method than on the cut-drop method.

We conclude this subsection with a mesh (see Figure 13) originally generated with Pointwise [29] that is normally used for hypersonic flow of re-entry vehicles in the Sandia Parallel Aerodynamics Reentry Code (SPARC) [13]. The computational domain corresponds to the space surrounding the vehicle with finer mesh resolution as one approaches the vehicle surface (i.e., cylindrical cavity) and the nose cone to resolve boundary layers. The discrete matrix  $A$  is  $4,298,409 \times 4,298,409$  and the Dirichlet surface corresponds to the yellow horseshoe shaped face furthest from the cone. Table 5 gives the iteration counts and AMG operator complexities. A dash

$\theta$	A/SA/Val			A/Sng/Val			DLap/SA/Val			DLap/Sng/Val			SLap/SA/Gap		
	SL	DL	$\alpha$	SL	DL	$\alpha$	SL	DL	$\alpha$	SL	DL	$\alpha$	SL	DL	$\alpha$
.01	-	-	-	-	-	-	99	46	1.42	46	45	2.28	166	161	2.16
.02	-	-	-	-	-	-	114	50	1.42	36	33	2.36	151	146	2.56
.04	-	-	-	-	-	-	240	68	1.45	31	27	2.14	122	124	2.54
.08	-	-	-	-	-	-	318	120	1.49	51	21	2.31	101	101	2.46
.16	-	-	-	-	-	-	202	244	1.45	76	13	2.37	77	76	2.40
.32	-	481	1.39	100	98	1.56	300	290	1.38	46	12	2.29	53	49	3.33

TABLE 5

Iteration counts and AMG operator complexities  $\alpha$  for standard lumping SL and distributed lumping DL on HIFiRE-1 mesh problem.

indicates that a particular run did not converge within 500 iterations. As with previous results, using  $A$  as the SOC matrix generally leads to failure. The DLap/SA/Val results with diagonal lumping are somewhat disappointing, but they improve noticeably with distributed lumping. Further, DLap/SA/Val gives by far the best operator complexities. Thus, if storage is a concern, this method combined with a low tolerance could be attractive. We note that  $\theta = .01$  is indeed a fairly good choice for this problem as with  $\theta = .001$  (not shown here), the iteration counts rise to 70 iterations with distributed lumping. In terms of convergence, however, the overall best method

is with  $\text{DLap/Sgn/Val}$  in conjunction with distributed lumping. In particular, with  $\theta \geq .16$  the number of required iterations is more than three times less than the best option with  $\text{DLap/SA/Val}$ . Once again, distributed lumping has a major impact for  $\text{DLap/SA/Val}$  and  $\text{DLap/Sgn/Val}$ , while having little influence on  $\text{DLap/SA/Gap}$ . Finally, we note that the best  $\theta$  choice for  $\text{DLap/Sgn/Val}$  and  $\text{DLap/SA/Gap}$  is relatively consistent across all problems considered in this manuscript, while the best  $\theta$  choice varies significantly for  $\text{DLap/SA/Val}$ , making it more problematic to define default  $\theta$  values for users who do not wish to tune parameters.

**5. Conclusions and Future Work.** We have studied strong and weak AMG classification when solving Poisson problems on stretched meshes using linear finite elements. We have centered our study on the choice of SOC matrix, the scaling applied to the SOC matrix entries, and whether or not it is best to classify based solely on a threshold or whether it can be advantageous to instead look for gaps in the scaled SOC entries. Additionally, we have defined a new distributed lumping procedure to account for dropped/weak entries. Under modest assumptions, this new lumping procedure is guaranteed to not reverse the sign of diagonal entries in the discretization matrix, which could have serious detrimental convergence effects. Overall, we find that the best algorithm combination for Poisson problems uses a distance Laplacian operator to define the SOC matrix together with a non-symmetric scaling scheme, which is normally used in classical AMG as opposed to smoothed aggregation AMG. In conjunction with thresholds  $\theta \geq .08$  and distributed lumping, this combination performed consistently well on finite element discretized Poisson problems defined over a wide range of meshes. Generally, we found that fairly high thresholds also performed well for  $\text{DLap/SA/Gap}$ . While the best  $\theta$  choice for a more traditional smoothed aggregation criteria using either  $A$  or a distance Laplacian SOC matrix could vary significantly. The relatively consistent best- $\theta$  choice for  $\text{DLap/Sgn/Val}$  and  $\text{DLap/SA/Gap}$  is due to the way in which they leverage the largest magnitude off-diagonal entry of the distance Laplacian within each row. In particular, both schemes guarantee that this entry is labeled strong along with other entries whose magnitude is *close* to this largest-magnitude entry. Overall, proper classification has a significant impact on AMG convergence with the best performing variants requiring 10's of iterations while poor performing variants might require 100's of iterations or not even converge.

The main limitation in this study is that the distance Laplacian is mostly appropriate for diffusion dominated systems without significant material variations. An archive version of the paper *Smoothed aggregation algebraic multigrid for problems with heterogeneous and anisotropic materials*, by Fimbach, Phillips, Glusa, Popp, Siefert, and Mayr will appear shortly. This paper generalizes the distance Laplacian idea to problems with material variation. A second paper is in the planning phase which focuses on defining a SOC matrix by developing a crude approximation to  $M^{-1}A$  where  $M$  is the finite element mass matrix and  $A$  is the finite element stiffness matrix. These approaches are somewhat complementary and are both intended to address limitations of the distance Laplacian. We also plan to further adapt and evaluate the distributed lumping scheme to more complex partial differential equations.

**Appendix A. 2D Quadrilateral Under Uniaxial Stretch.** Consider a 2D structured mesh where the  $y$ -direction is stretched by a constant factor  $\alpha$ , relative to the mesh spacing in the  $x$ -direction,  $h$ . Discretization of a Poisson operator by first

order nodal quadrilateral elements yields the element stiffness matrix

$$(A.1) \quad \frac{1}{6\alpha} \begin{bmatrix} 2\alpha^2 + 2 & -2\alpha^2 + 1 & -\alpha^2 - 1 & \alpha^2 - 2 \\ -2\alpha^2 + 1 & 2\alpha^2 + 2 & \alpha^2 - 2 & -\alpha^2 - 1 \\ -\alpha^2 - 1 & \alpha^2 - 2 & 2\alpha^2 + 2 & -2\alpha^2 + 1 \\ \alpha^2 - 2 & -\alpha^2 - 1 & -2\alpha^2 + 1 & 2\alpha^2 + 2 \end{bmatrix}$$

whose  $(i, j)$  entries are defined by  $\int \nabla \phi_j \cdot \nabla \phi_i \, d\Omega_e$  where  $\phi_k$  is the  $k^{th}$  vertex basis function,  $\Omega_e$  is the stretched element, and vertices are ordered in a counter-clockwise fashion starting at the  $(-1, -1)$  node on the reference element. This can be converted to an interior vertex stencil by noting that four elements contribute to the stencil central point while two elements contribute to the stencil sides, leading to the stencil

$$(A.2) \quad \frac{1}{6\alpha} \begin{pmatrix} -1 - \alpha^2 & -4 + 2\alpha^2 & -1 - \alpha^2 \\ 2 - 4\alpha^2 & 8 + 8\alpha^2 & 2 - 4\alpha^2 \\ -1 - \alpha^2 & -4 + 2\alpha^2 & -1 - \alpha^2 \end{pmatrix}.$$

Here, identical stencil values are highlighted with identical dotted rectangles, dotted ovals, or solid ovals. Figure 14 plots the corresponding traditional SA criterion values.

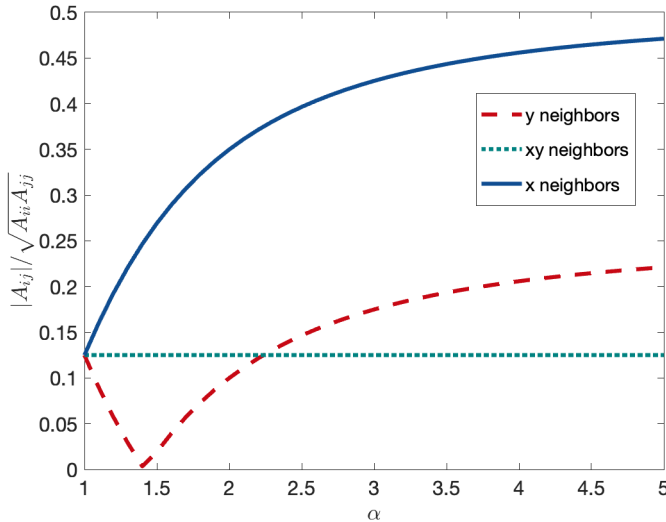


FIG. 14. Traditional SA criterion values for 2D stretched stencil.

To label nearby  $x$  neighbors as strong and label distant  $xy$  and  $y$  neighbors as weak requires a threshold greater than .25 but less than .5 when  $\alpha$  is large. Unfortunately, this threshold would then label all off-diagonals as weak when  $\alpha \approx 1$ .

Figure 15 depicts results using distributed lumping for the 2D stretched mesh and is the counterpart to Figure 5 which uses diagonal lumping. The two figures are similar, but one can identify cases where distributed lumping improves the convergence (e.g., the speckled dots appearing for DLap/Sgn/Val for  $\theta = .16$  and .32 no longer appear speckled with distributed lumping).

## Appendix B. Element Stencil: 3D Hexahedron Under Uniaxial Stretch.

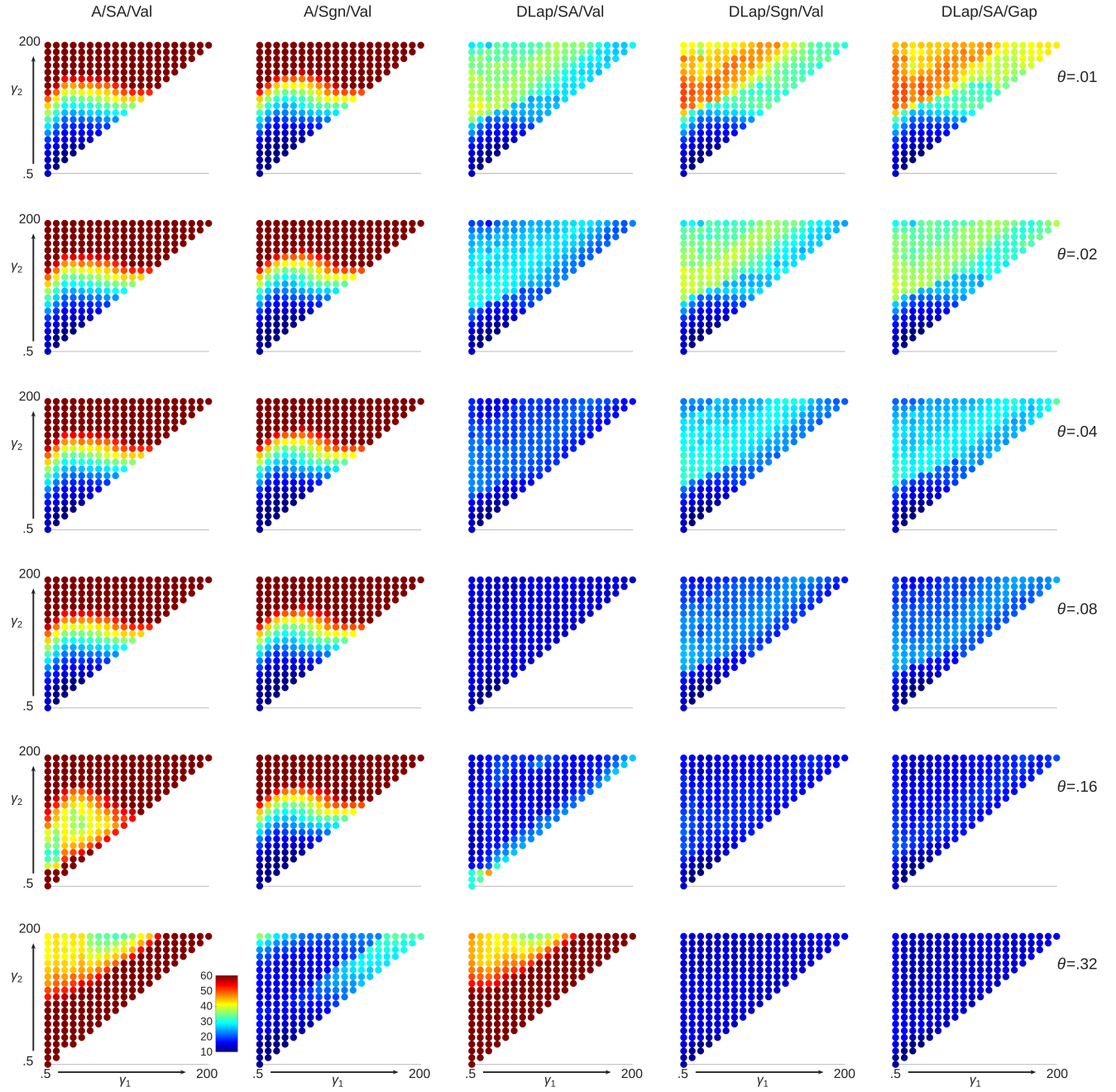


FIG. 15. Iterations  $\times$  operator complexity, with the color scale from 10 to 60 for the 3D mesh. Columns represent algorithm choices (described in Section 4.1) and rows represent tolerances,  $\theta$ . Distributed lumping is use for all experiments. See Section 4.1.

Consider a 3D structured mesh where the  $z$ -direction is stretched by a constant factor  $\alpha$  relative to the mesh spacing  $h$  in the  $x$ - and  $y$ -directions. Discretization of a Poisson operator by first order nodal finite elements on a hexahedral mesh yields the element stiffness matrix

$$(B.1) \quad \frac{h}{18\alpha} \begin{bmatrix} 4\alpha^2 + 2 & -\alpha^2 + 1 & -2\alpha^2 + \frac{1}{2} & -\alpha^2 + 1 & 2\alpha^2 - 2 & -\frac{\alpha^2}{2} - 1 & -\alpha^2 - \frac{1}{2} & -\frac{\alpha^2}{2} - 1 \\ -\alpha^2 + 1 & 4\alpha^2 + 2 & -\alpha^2 + 1 & -2\alpha^2 + \frac{1}{2} & -\frac{\alpha^2}{2} - 1 & 2\alpha^2 - 2 & -\frac{\alpha^2}{2} - 1 & -\alpha^2 - \frac{1}{2} \\ -2\alpha^2 + \frac{1}{2} & -\alpha^2 + 1 & 4\alpha^2 + 2 & -\alpha^2 + 1 & -\alpha^2 - \frac{1}{2} & -\frac{\alpha^2}{2} - 1 & 2\alpha^2 - 2 & -\frac{\alpha^2}{2} - 1 \\ -\alpha^2 + 1 & -2\alpha^2 + \frac{1}{2} & -\alpha^2 + 1 & 4\alpha^2 + 2 & -\frac{\alpha^2}{2} - 1 & -\alpha^2 - \frac{1}{2} & -\frac{\alpha^2}{2} - 1 & 2\alpha^2 - 2 \\ 2\alpha^2 - 2 & -\frac{\alpha^2}{2} - 1 & -\alpha^2 - \frac{1}{2} & -\frac{\alpha^2}{2} - 1 & 4\alpha^2 + 2 & -\alpha^2 + 1 & -2\alpha^2 + \frac{1}{2} & -\alpha^2 + 1 \\ -\frac{\alpha^2}{2} - 1 & 2\alpha^2 - 2 & -\frac{\alpha^2}{2} - 1 & -\alpha^2 - \frac{1}{2} & -\alpha^2 + 1 & 4\alpha^2 + 2 & -\alpha^2 + 1 & -2\alpha^2 + \frac{1}{2} \\ -\alpha^2 - \frac{1}{2} & -\frac{\alpha^2}{2} - 1 & 2\alpha^2 - 2 & -\frac{\alpha^2}{2} - 1 & -2\alpha^2 + \frac{1}{2} & -\alpha^2 + 1 & 4\alpha^2 + 2 & -\alpha^2 + 1 \\ -\frac{\alpha^2}{2} - 1 & -\alpha^2 - \frac{1}{2} & -\frac{\alpha^2}{2} - 1 & 2\alpha^2 - 2 & -\alpha^2 + 1 & -2\alpha^2 + \frac{1}{2} & -\alpha^2 + 1 & 4\alpha^2 + 2 \end{bmatrix}$$

where  $\Omega_e$  is the stretched element and degrees of freedom are ordered in a front-to-back, counter-clockwise fashion starting at the  $(-1, -1, -1)$  node on the reference element. This can be converted into an interior stencil by viewing the stencil as a cube and noting that stencil central point has eight element contributions, the six stencil values associated with face centers have two element contributions, the twelve stencil values associated with edge centers have four element contributions, while the eight stencil values associated with corners have one element contribution. This yields the stencil depicted in Figure 1.

### Appendix C. Pamgen Mesh Generation Templates.

**C.1. 2D Stretched Brick Mesh.** Section 4.1 meshes are generated with the following Pamgen [12] template:

```
mesh
  brick
  numx 3
    xblock 1 1.0, interval 10
    xblock 2 {3.0*(GAMMA1+1)}, first size .1, last size {GAMMA1/10}
    xblock 3 {GAMMA1}, interval 10
  numy 3
    yblock 1 1.0, interval 10
    yblock 2 {3.0*(GAMMA2+1)}, first size .1, last size {GAMMA2/10}
    yblock 3 {GAMMA2}, interval 10
  end
  set assign
    sideset, jlo, 2
  end
end
```

Braces denote preprocessor substitution and the variables GAMMA1 and GAMMA2 are varied logarithmically between 0.5 and 200.

**C.2. 3D Stretched Brick Mesh.** Section 4.2 meshes are generated with the following Pamgen template:

```

mesh
brick
numx 3
  xblock 1 1.0, interval 10
  xblock 2 {3.0*(GAMMA1+1)}, first size .1, last size {GAMMA1/10}
  xblock 3 {GAMMA1}, interval 10
numy 3
  yblock 1 1.0, interval 10
  yblock 2 {3.0*(GAMMA2+1)}, first size .1, last size {GAMMA2/10}
  yblock 3 {GAMMA2}, interval 10
numz 1
  zblock 1 8.0, interval 80
end
set assign
  sideset, jlo, 2
end
end

```

**C.3. 3D Radial Trisection Mesh.** Section 4.3 meshes are generated with the following Pamgen template:

```

mesh
radial trisection
  trisection blocks, {GAMMA2}
  transition radius, 6.
  numz 1
  zblock 1 20. interval 20
  numr 2
  rblock 1 8.0 interval 4
  rblock 2 {200*floor((1+GAMMA1)/2)} first size 1.0 last size {GAMMA1}
  numa 1
  ablock 1 90. interval 24
end
set assign
  sideset, ihi, 4
end
end

```

The variable `GAMMA2` indicates the number of trisection blocks. The variable `GAMMA1` is varied logarithmically up to 100, depending on the number of trisection blocks (this is due to limits of Pamgen). For one, two, three, four and six blocks, `GAMMA1` correspondingly begins at 1.0658, 1.1875, 1.3231, 1.4742 and 1.6426.

## REFERENCES

- [1] T. BLACKER, S. J. OWEN, M. L. STATEN, R. W. QUADROS, B. HANKS, B. CLARK, R. J. MEYERS, C. ERNST, K. MERKLEY, R. MORRIS, C. McBRIDE, C. STIMPSON, M. PLOOSTER, AND S. SHOWMAN, *CUBIT: Geometry and mesh generation toolkit, 15.2 user documentation*, Tech. Report SAND2016-1649 R, Sandia National Laboratory, 2016.
- [2] A. BRANDT, *General highly accurate algebraic coarsening*, Electronic Transactions on Numerical Analysis, 10 (2000), pp. 1–20.
- [3] A. BRANDT, J. BRANNICK, K. KAHL, AND I. LIVSHITS, *Algebraic distance for anisotropic diffusion problems: multilevel results*, Electronic Transactions on Numerical Analysis, 44 (2015), pp. 472–496.

- [4] A. BRANDT, S. MCCORMICK, AND J. RUGE, *Algebraic multigrid (AMG) for sparse matrix equations*, in Sparsity and its applications, D. Evans, ed., Cambridge University Press, Cambridge, 1984, pp. 257–284.
- [5] J. BRANNICK, M. BREZINA, S. MACLACHLAN, T. MANTEUFFEL, AND S. MCCORMICK, *An energy-based AMG coarsening strategy*, Numerical Linear Algebra with Applications, 13 (2006), pp. 133–148.
- [6] J. BRANNICK, F. CAO, K. KAHL, R. D. FALGOUT, AND X. HU, *Optimal interpolation and compatible relaxation in classical algebraic multigrid*, SIAM Journal on Scientific Computing, 40 (2018), pp. A1473–A1493.
- [7] J. BRANNICK AND L. ZIKATANOV, *Algebraic multigrid methods based on compatible relaxation and energy minimization*, in Domain Decomposition Methods in Science and Engineering XVI, O. Widlund and D. E. Keyes, eds., vol. 55 of Lecture Notes in Computational Science and Engineering, Springer, Berlin, 2007, pp. 15–26.
- [8] J. J. BRANNICK AND R. D. FALGOUT, *Compatible relaxation and coarsening in algebraic multigrid*, SIAM J. Sci. Comput., 32 (2010), pp. 1393–1416.
- [9] P. BROWN, R. FALGOUT, AND J. JONES, *Semicoarsening multigrid on distributed memory machines*, SIAM J. Sci. Comput., 21 (2000), pp. 1823–1834.
- [10] J. DENDY, *Black box multigrid*, J. Comp. Phys., 48 (1982), pp. 366–386.
- [11] J. DENDY, M. IDA, AND J. RUTLEDGE, *A semicoarsening multigrid algorithm for SIMD machines*, SIAM J. Sci. Stat. Comput., 13 (1992), pp. 1460–1469.
- [12] D. HENSINGER, R. DRAKE, J. FOUCAR, AND T. GARDINER, *Pamgen, a library for parallel generation of simple finite element meshes*, Tech. Report SAND2008-1933, Sandia National Laboratories, 2008.
- [13] M. HOWARD, T. FISHER, M. HOEMMEN, D. DINZL, J. OVERFELT, A. BRADLEY, K. KIM, AND S. RAJAMANICKAM, *Employing multiple levels of parallelism for CFD at large scales on next generation high-performance computing platforms*, in Proceedings of ICCFD10, 2018, pp. ICCFD10-079, <https://www.iccfd.org/iccfd10/proceedings.html>.
- [14] J. HU, C. SIEFERT, AND R. TUMINARO, *Smoothed aggregation for difficultly stretched mesh and coefficient variation problems*, Numer. Lin. Alg. Appl., 29 (2022).
- [15] O. LIVNE, *Coarsening by compatible relaxation*, Numerical Linear Algebra with Applications, 11 (2004), pp. 205–227.
- [16] D. MAVRIPLIS, *Multigrid strategies for viscous flow solvers on anisotropic unstructured meshes*, Journal of Computational Physics, 145 (1998), pp. 141–165.
- [17] Y. NOTAY AND P. S. VASSILEVSKI, *Recursive krylov-based multigrid cycles*, Numerical Linear Algebra with Applications, 15 (2008), pp. 473–487.
- [18] L. OLSON, J. SCHRODER, AND R. TUMINARO, *New perspective on strength measures in algebraic multigrid*, Numer. Linear Algebra Appl., 17 (2010), pp. 713–733.
- [19] A. PROKOPENKO, J. J. HU, T. A. WIESNER, C. M. SIEFERT, AND R. S. TUMINARO, *MueLu user's guide 1.0*, Tech. Report SAND2014-18874, Sandia National Laboratories, 2014.
- [20] J. RUGE AND K. STÜBEN, *Algebraic multigrid (AMG)*, in Multigrid Methods, S. McCormick, ed., vol. 3 of Frontiers in Applied Mathematics, SIAM, Philadelphia, 1985, pp. 73–130.
- [21] M. SALA, P. LIN, R. TUMINARO, AND J. SHADID, *Algebraic multilevel preconditioners for non-symmetric PDEs on stretched grids*, in Domain Decomposition Methods in Science and Engineering XVI, O. B. Widlund and D. E. Keyes, eds., vol. 55 of Lecture Notes in Computational Science and Engineering, Springer-Verlag, 2006, pp. 739–746.
- [22] S. SCHAFFER, *A semicoarsening multigrid method for elliptic partial differential equations with highly discontinuous and anisotropic coefficients*, SIAM J. Sci. Comput., 20 (1998), pp. 228–242.
- [23] D. STEPHAN, *Sierra low mach module: Nalu theory manual 1.0*, Tech. Report SAND2015-3107W, Sandia National Laboratory, 2015, <https://github.com/NaluCFD/NaluDoc>.
- [24] S. R. TIESZEN, S. P. DOMINO, AND A. R. BLACK, *Validation of a simple turbulence model suitable for closure of temporally-filtered Navier-Stokes Equations using a helium plume*, Tech. Report SAND2005-3210, Sandia National Laboratory, 2005.
- [25] R. TUMINARO AND C. TONG, *Parallel smoothed aggregation multigrid: Aggregation strategies on massively parallel machines*, in SuperComputing 2000 Proceedings, J. Donnelley, ed., 2000.
- [26] P. VANĚK, M. BREZINA, AND J. MANDEL, *Convergence of algebraic multigrid based on smoothed aggregation*, Numer. Math., 88 (2001), pp. 559–579.
- [27] P. VANĚK, J. MANDEL, AND M. BREZINA, *Algebraic multigrid based on smoothed aggregation for second and fourth order problems*, Computing, 56 (1996), pp. 179–196.
- [28] A. VORONIN, S. MACLACHLAN, L. N. OLSON, AND R. S. TUMINARO, *Monolithic algebraic multigrid preconditioners for the stokes equations*, SIAM Journal on Scientific Computing, 47

(2025), pp. A343–A373.

[29] C. D. WOEBER, E. J. S. GANTT, AND N. J. WYMAN, *Mesh generation for the NASA high lift common research model (hl-crm)*, 3rd AIAA High Lift Prediction Workshop and 1st AIAA Geometry and Mesh Generation Workshop, (2017), <https://commonresearchmodel.larc.nasa.gov/wp-content/uploads/sites/7/2018/01/AIAA-2017-0363.pdf>. Held at the AIAA SciTech Forum, Grapevine, TX, USA, 9-13 January 2017. AIAA Paper 2017-0363.